

# Spin oscillations of neutrinos scattered by the supermassive black hole in the galactic center

Mridupawan Deka<sup>1)\*</sup> and Maxim Dvornikov<sup>1),2)†</sup>

<sup>1)</sup> *Bogoliubov Laboratory of Theoretical Physics,  
Joint Institute for Nuclear Research, Dubna, Russia;*

<sup>2)</sup> *Pushkov Institute of Terrestrial Magnetism,  
Ionosphere and Radiowave Propagation (IZMIRAN), Troitsk, Moscow, Russia*

Abstract

In this work, we study the propagation and spin oscillations of neutrinos in their scattering by a supermassive black hole (SMBH) surrounded by a realistic accretion disk. We use a semi-analytical model of a thick accretion disk which can co-rotate and counter-rotate with respect to BH. Moreover, we assume that a disk contains only a toroidal magnetic field of moderate strength. Spin precession of neutrinos, which are supposed to be Dirac particles, is caused by the interaction of the neutrino magnetic moment with the magnetic field in the disk. We consider the incoming flux of neutrinos having an arbitrary angle with respect to the BH spin since the recent results of the Event Horizon Telescope indicate that the BH spin in the galactic center is not always perpendicular to the galactic plane. For our study, we consider a large number of incoming test neutrinos. We briefly discuss our results and their applications in the observations of astrophysical neutrinos.

## I. INTRODUCTION

Neutrinos are a unique tool to explore the laws of nature because their nonzero masses and mixing between flavors open a window to the physics beyond the standard model. The extremely weak opacity of matter for neutrinos allows one to use such particles to probe various structures which cannot be observed with help of electromagnetic radiation. This high penetrability is of great importance for astrophysical neutrinos. Sizable efforts are made in Refs. [1, 2] to detect neutrinos arriving on Earth from outside the solar system. Moreover the attempts to observe multimessenger astronomy effects involving neutrinos are undertaken, e.g., in Ref. [3].

The observation of a neutrino in a detector is nontrivial because of both rather weak strength of interaction with a target and the additional feature which results from the fact that neutrinos

---

\* [mpdeka@theor.jinr.ru](mailto:mpdeka@theor.jinr.ru)

† [maxim.dvornikov@gmail.com](mailto:maxim.dvornikov@gmail.com)

participate in electroweak interactions where parity is violated. The neutrino interaction cross-section depends on the neutrino helicity: left-handed neutrinos are active whereas right-handed ones are sterile. Thus, if the spin of a neutrino is flipped owing to the particle interaction with external fields, we will observe the reduction of the initial neutrino flux. If this process happens within one neutrino generation, it is called neutrino spin oscillations. Originally, neutrino spin oscillations were associated with non-trivial neutrino electromagnetic properties, i.e. the possibility for a neutrino to possess a nonzero magnetic moment [4]. In this situation, the neutrino spin-flip happens in an external magnetic field [5].

Other interactions, including the gravitational one, can also contribute to the spin precession of a particle. The problem of a spinning body motion in a gravitational field was studied, first, in Ref. [6]. The review of the extensive literature on the classical and quantum approaches for the description of spinning particles in gravitational fields and non-inertial frames is present in Ref. [7]. Neutrino spin oscillations under the influence of a gravitational field are studied in our works [8, 9] based on the quasiclassical approach. The formalism developed in Refs. [8, 9] is then applied in Refs. [10–14] to study neutrino spin oscillations in various extensions of the General Relativity (GR).

In Refs. [15–19], we have applied the quasiclassical formalism for the studies of spin effects in the neutrino gravitational scattering by a black hole (BH) surrounded by a realistic magnetized accretion disk. First, the neutrino in- and out-states are well defined from the point of view of the quantum field theory in this kind formulation of the problem. Second, this research has been inspired by the recent observations of the silhouettes of the event horizons of supermassive BHs (SMBH) in the centers of M87 [20] and the Milky Way [21]. This achievement of the observational astronomy is a unique test of GR in the strong field limit [22].

Some accretion disks around BHs are proposed in Ref. [23] to emit high energy neutrinos. These particles move in strong gravitational fields in the vicinity of the BHs. The spin of such neutrinos can precess in the external fields present in the accretion disk. It will lead to the modification of the disk image seen in a neutrino telescope compared to the optical one obtained, e.g., in Ref. [24]. Indeed, some of the neutrinos can become right-handed owing to spin oscillations. Thus, certain regions of a disk will be invisible.

Another possibility for the manifestation of the spin effects in the neutrino gravitational scattering is when, e.g., supernova (SN) neutrinos are gravitationally lensed by the SMBH in the center of our Galaxy. In this situation, we can observe the reduction of the estimated neutrino flux if the Earth is at certain position with respect to SN and the galactic center. This kind of process is

studied, e.g., in Ref. [25].

In the present work, we continue our studies of spin oscillations of neutrinos gravitationally scattered by a BH. Similar to the Refs. [18, 19], we consider a rotating SMBH. Following the ‘‘Polish doughnut’’ model in Ref. [27], we introduce a thick magnetized accretion disk surrounding the SMBH. In the present work, we assume that the disk contains only the toroidal magnetic field [28] unlike in Ref. [18, 19] where both toroidal and poloidal magnetic fields have been considered together.

This work differs from our previous works in the sense that here we consider the incoming neutrino beams traversing at a random angle with respect to the equatorial plane of the SMBH instead of traveling parallel to it. We consider a number of such incident angles in this study. This is motivated by the fact that the BH spin can be inclined towards the galactic plane in many cases. As an example, the spin of SMBH in our Galaxy is almost in the Galactic plane [26]. Since the relative position between a neutrino source and the Earth at the moment of the observation of neutrinos is not known, our study may shed light on the angle of inclination when the neutrinos are gravitationally scattered by such a BH. Furthermore, it also allows us to investigate whether there exists an inverse symmetry in the observed fluxes of neutrinos for the opposite values of the cosine of the incident angles while all parameters are kept fixed. The absence of such symmetry shall reveal the inherent feature of the metric.

Moreover, we consider the cases where the accretion disk is both co-rotating and counter-rotating with respect to the spin of the BH. If we observe a clear difference between the observed fluxes of scattered neutrinos for both the disks with the same combination of BH spin and incident angle, this may help in inferring the direction of the disk rotation in the measurement of astrophysical neutrinos.

Additionally in comparison to Ref. [18], we use a few million incoming test neutrinos, with the help of High Performance Parallel Computing, to significantly increase the resolution of fluxes of the scattered neutrinos.

This work is organized as follows: In Sec. II, we briefly describe our study. In Sec. III, we discuss the trajectory of a test particle in the gravitational field of a rotating BH. The spin evolution of the test particle along this trajectory is discussed in Sec IV. The interactions of the magnetic moment of neutrinos with the toroidal magnetic fields and background matter are discussed. In Sec. V, we discuss the model of the magnetized accretion disks that we use in this work. We define all the parameters needed to describe the disk. We also briefly discuss the definitions of both the co-rotating and counter-rotating disks. The numerical parameters are chosen in Sec. VI. We

discuss our results in Sec. VII with a conclusion of our work given in Sec. VIII.

## II. FORMALISM

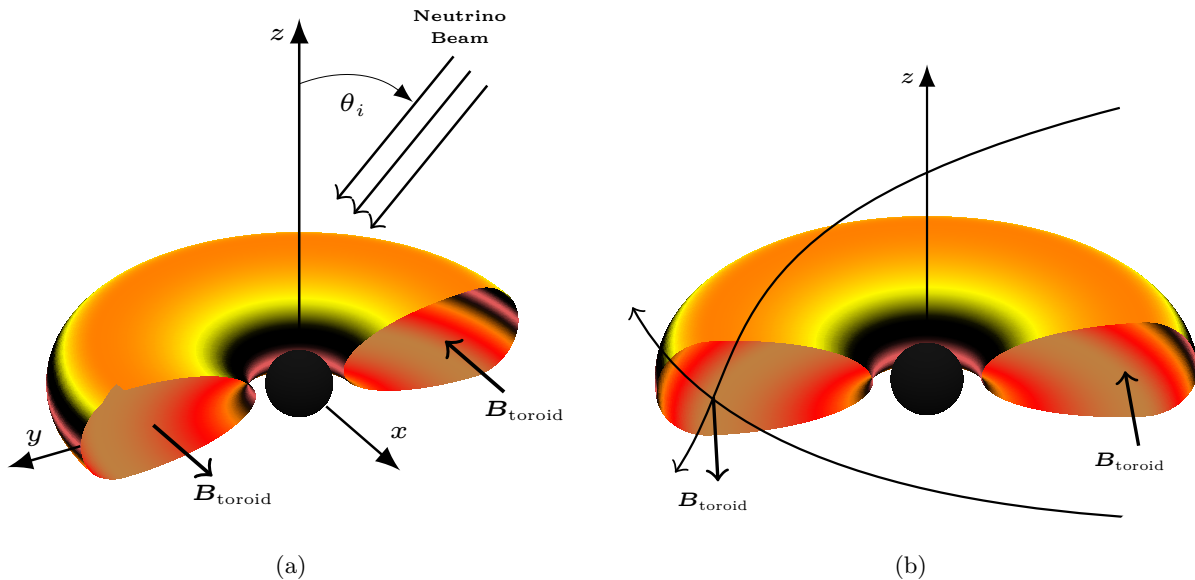


FIG. 1. Schematic diagrams showing neutrino trajectories. (a) A beam of neutrinos coming from  $\infty$  at an angle  $\theta_i$  with respect to the equatorial plane of a spinning BH. (b) Neutrinos crossing the equatorial plane through the accretion disk. The toroidal magnetic field is perpendicular to their momenta.

We first consider that a beam of Dirac left-handed neutrinos is emitted by a distant source. These neutrinos approach a spinning SMBH with a polar angle  $\theta_i$  with respect to the equatorial plane of the SMBH such that their initial co-ordinates can be written as  $(r, \theta, \phi)_s = (\infty, \theta_i, 0)$ ; cf. Fig. 1(a). Some of the neutrinos are captured by the BH due to the gravitational pull. The rest are then scattered gravitationally.

Note that we are not phenomenologically interested in the situations when a neutrino is captured by the BH, and it keeps rotating around it. Even if spin oscillations occur for such a neutrino, it cannot be detected by a remote observer. We can study the situation when a beam of neutrinos is scattered by the BH, and one measures the polarization of incoming and outgoing particles which are in the flat space-time asymptotically.

Since we assume that a neutrino has a nonzero magnetic moment  $\mu$ , the scattered beam of neutrinos experiences electromagnetic interactions with the toroidal magnetic field of the accretion disk (See Fig. 1(b)). It also experiences electroweak interactions with the background matter fields in the accretion disk. These interactions cause neutrino spin precession resulting in spin oscillations. This

implies that some of the left-handed neutrinos become right-handed or sterile.

The gravitationally scattered neutrinos escape to infinity. Since some of these neutrinos are likely sterile, not all of them can be observed at the observer position,  $(r, \theta, \phi)_{\text{obs}} = (\infty, \theta_{\text{obs}}, \phi_{\text{obs}})$ . Our goal is to study the probability distributions of the left-handed neutrinos remaining left handed as functions of  $\theta_{\text{obs}}$  and  $\phi_{\text{obs}}$ . In the following, we derive the trajectories and spin evolution of these neutrinos between  $(r, \theta, \phi)_s$  and  $(r, \theta, \phi)_{\text{obs}}$ .

### III. TRAJECTORIES OF ULTRA-RELATIVISTIC NEUTRINOS IN KERR SPACETIME

In this section, we shall describe the trajectories of ultra-relativistic neutrinos in the presence of the gravitational field of a spinning BH. The spacetime in this case is defined using Kerr metric. In Boyer-Lindquist coordinates,  $x^\mu = (t, r, \theta, \phi)$ , the Kerr metric for a BH with mass  $M$  and angular momentum  $J$  along the  $z$ -axis can be written as,

$$ds^2 = g_{\mu\nu} dx^\mu dx^\nu = \left(1 - \frac{rr_g}{\Sigma}\right) dt^2 + 2\frac{rr_g a \sin^2 \theta}{\Sigma} dt d\phi - \frac{\Sigma}{\Delta} dr^2 - \Sigma d\theta^2 - \frac{\Xi}{\Sigma} \sin^2 \theta d\phi^2, \quad (1)$$

where,

$$\Delta = r^2 - rr_g + a^2, \quad \Sigma = r^2 + a^2 \cos^2 \theta, \quad \Xi = (r^2 + a^2) \Sigma + rr_g a^2 \sin^2 \theta. \quad (2)$$

Here,  $r_g = 2M$  is the Schwarzschild radius, and  $J = aM$  where  $0 < a < M$ .

The geodesic motion of an ultra-relativistic test particle in Kerr metric has three constants of motion,

$E$ : The total energy of the particle.

$L$ : The projection of the angular momentum of the particle on the BH spin.

$Q$ : The Carter constant.

In this study,  $Q > 0$  since, here, we are considering the scattering of particles only [29].

The trajectory of an ultra-relativistic particle in the presence of the gravitational field of a spinning BH can be written in terms of two integral equations as [30],

$$\int \frac{dr}{\pm\sqrt{R}} = \int \frac{d\theta}{\pm\sqrt{\Theta}}, \quad (3)$$

$$\phi = a \int \frac{dr}{\pm\Delta\sqrt{R}} [(r^2 + a^2)E - aL] + \int \frac{d\theta}{\pm\sqrt{\Theta}} \left[ \frac{L}{\sin^2 \theta} - aE \right], \quad (4)$$

where  $R$  and  $\Theta$  potentials are defined as,

$$R(r) = [(r^2 + a^2)E - aL]^2 - \Delta[Q + (L - aE)^2], \quad (5)$$

$$\Theta(\theta) = Q + \cos^2 \theta \left( a^2 E^2 - \frac{L^2}{\sin^2 \theta} \right). \quad (6)$$

We choose  $\pm$  signs for  $\sqrt{R}$  and  $\sqrt{\Theta}$  in Eqs. (3) and (4) to be the same as those of  $dr$  and  $d\theta$  depending upon whether a neutrino is approaching from or moving away to infinity, e.g. if a neutrino is approaching from infinity towards the BH, we choose  $-ve$  sign for the  $r$ -integral. Similarly, we choose  $+ve$  sign if it is moving away to infinity. When the neutrino is approaching the BH, the value of  $\theta$  either decreases (minimum being 0) or increases (maximum being  $\pi$ ). We choose  $-ve$  sign for the  $\theta$ -integral in the first case and  $+ve$  sign for the second case. For computational convenience, we designate the neutrinos in the first case as the ‘‘Upper’’ neutrinos. The neutrinos in the second case is designated as the ‘‘Lower’’ neutrinos. This kind of separation of particles is equivalent to the choice of the initial condition.

For the purpose of computation, we now define the following dimensionless variables such that,

$$r = xr_g, L = yr_g E, Q = wr_g^2 E^2, a = zr_g, t = \cos \theta. \quad (7)$$

From now on all our expressions will be dimensionless.

Using Eq. (7), we can rewrite Eqs. (3) and (4) as,

$$z \int \frac{dx}{\pm \sqrt{R(x)}} = \int \frac{dt}{\pm \sqrt{\Theta(t)}}, \quad (8)$$

$$\phi = z \int \frac{(x - zy)dx}{\pm \sqrt{R(x)}(x^2 - x + z^2)} + \frac{y}{z} \int \frac{dt}{\pm \sqrt{\Theta(t)}(1 - t^2)}, \quad (9)$$

where,

$$R(x) = (x^2 + z^2 - yz)^2 - (x^2 - x + z^2) [w + (z - y)^2], \quad (10)$$

$$\Theta(t) = (t_-^2 + t^2)(t_+^2 - t^2), \quad (11)$$

$$t_{\pm}^2 = \frac{1}{2z^2} \left[ \sqrt{(z^2 - y^2 - w)^2 + 4z^2 w} \pm (z^2 - y^2 - w) \right], \quad (12)$$

with  $t_{\pm}^2 > 0$ . The value of the variable,  $t$ , as a function of  $x$  in Eq. (8) oscillates between  $\pm t_+$ ,  $-t_+ < t < +t_+$ .

Note that not all the trajectories defined by Eqs. (3) and (4) are going to survive since some of the particles get captured by the BH and fall into it. The edge between the captured and escaped particles satisfy the conditions,  $R(\tilde{r}) = R'(\tilde{r}) = 0$ . These conditions lead to the parametric

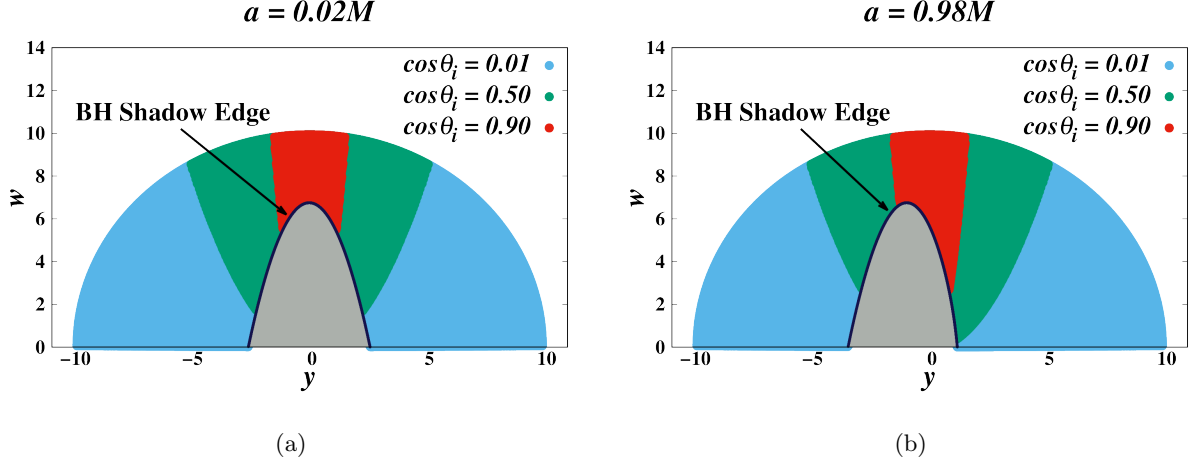


FIG. 2. Figures showing the values of the integrals of motion for the captured and escaped ultra-relativistic neutrinos together with the BH shadow. Areas that are not gray are the accepted values of  $L/E$  and  $\sqrt{Q}/E$  for three different values of  $t_i = \cos \theta_i$ , namely  $t_i = 0.01, 0.50$  and  $0.90$ . (a)  $a = 0.02M$  and (b)  $a = 0.98M$ .

equations in terms of the following dimensionless variables as,

$$y = -\frac{1}{z(2x-1)} [x^2(2x-3) + z^2(2x+1)], \quad (13)$$

$$w = \frac{x^3}{z^2(2x-1)^2} [8z^2 - x(2x-3)^2], \quad (14)$$

$$x_{\pm} = 1 + \cos \left[ \frac{2}{3} \arccos(\pm 2z) \right], \quad x_- < x < x_+. \quad (15)$$

The parametric Eqs. (13)-(15) define the BH shadow curve between the captured and escaped particles. In Figs. 2(a) and 2(b), we show BH shadow curves for the two cases of BH spin,  $a = 0.02M$  and  $a = 0.98M$ , respectively. The shadow areas seen by an observer can be reconstructed using the results of, e.g., Ref. [30]. Those trajectories, which correspond to the gray areas, are discarded from the computation.

In our previous works, e.g., in Ref. [18], we considered the flux of incoming neutrinos which is parallel to the equatorial plane. In the present work, we study the situation when the incoming flux is still uniform. However, the angle between the axis of the flux at  $r \rightarrow \infty$  and the BH spin is arbitrary,  $0 < \theta_i < \pi$ ; cf. Fig. 1(a).

The arbitrary,  $t_i = \cos \theta_i \neq 0$ , means that  $\Theta > 0$  for any  $\theta_i$  in Eq. (5). This additional constraint can be rewritten as,

$$w > -z^2 t_i^2 + y^2 \frac{t_i^2}{1-t_i^2}. \quad (16)$$

In Figs. 2(a) and 2(b), we show the accepted values of  $y$  and  $w$  for three different values of  $t_i$ , namely  $t_i = 0.01, 0.50$  and  $0.90$ .

### A. Motion of the Upper Neutrinos

Let us first consider an upper neutrino approaching the BH from infinity. As mentioned earlier, the value of the variable,  $t$ , as a function of  $x$  in Eq. (8) oscillates between  $\pm t_+$ . We call the number of times when  $t$  reaches either  $-t_+$  or  $+t_+$  by the number of the inversions of the trajectory,  $N$ . On the other hand, we set the lower limit of  $x$  to be  $x > x_{\text{tp}}$ .  $x_{\text{tp}}$  is the turn point which is the maximal real root of the equation  $R(x) = 0$  with  $R(x)$  being given in Eq. (10). This is the minimal distance to the BH center. Generalizing the results of Ref. [19], we get the  $N$  for incoming neutrinos before they reach the turn point,  $x_{\text{tp}}$ , as,

$$N^{\text{before}} = \left\lfloor \frac{I_x - F_i}{2K} \right\rfloor + 1, \quad (17)$$

where,

$$F_i = F \left( \arccos \frac{t_i}{t_+}, \frac{t_+^2}{t_+^2 + t_-^2} \right), \quad (18)$$

is the Incomplete Elliptic integral of the first kind,  $\lfloor \dots \rfloor$  denotes the Floor function,  $K = K \left( \frac{t_+^2}{t_-^2 + t_+^2} \right)$  is the Complete Elliptic integral of first kind, and

$$I_x = z \sqrt{t_+^2 + t_-^2} \int_x^\infty \frac{dx'}{\sqrt{R(x')}}, \quad (19)$$

where  $x_{\text{tp}} < x < \infty$ . For the definitions of Elliptic integrals and functions, we follow those in Ref. [31]. Some of the useful expressions are given in Appendix A.

Using Eqs. (8) and (17), we can write the relation for  $\theta(x)$  for an incoming neutrino as,

$$\cos \theta_{\text{in}} = t_+ \text{cn} \left( (-1)^{N^{\text{before}}} \left\{ F_i - I_x + 4K \left\lfloor \frac{N^{\text{before}}}{2} \right\rfloor \right\} \middle| \frac{t_+^2}{t_-^2 + t_+^2} \right), \quad (20)$$

where  $\text{cn}(n|m)$  is the Elliptic Jacobi function.

Similarly using Eqs. (9), and (17), we can write the corresponding relation for the azimuthal angle  $\phi_{\text{in}}$  at the turn point as,

$$\phi_{\text{in}} = z \int_{x_{\text{tp}}}^\infty \frac{(x - zy)dx}{(x^2 - x + z^2)\sqrt{R(x)}} + \frac{y}{zt_-} \left\{ 2N^{\text{before}}\Pi - \Pi_i + (-1)^{N^{\text{before}}}\Pi_{\text{tp}} \right\}, \quad (21)$$

where  $t_{\text{tp}} = \cos \theta_{\text{tp}}$  at the turn point  $x_{\text{tp}}$ . We do not need the  $x$  dependence of  $\phi(x)$  along the whole trajectory. In Eq. (21),  $\Pi$  is the Complete Elliptic integral of third kind while  $\Pi_i$  and  $\Pi_{\text{tp}}$  are the Incomplete Elliptic integrals of third kind. They are denoted as follows,

$$\Pi = \Pi \left( t_+^2, -t_+^2/t_-^2 \right), \quad \Pi_i = \Pi \left( \arcsin(t_i/t_+), t_+^2, -t_+^2/t_-^2 \right), \quad \Pi_{\text{tp}} = \Pi \left( \arcsin(t_{\text{tp}}/t_+), t_+^2, -t_+^2/t_-^2 \right). \quad (22)$$

When the neutrino escapes to infinity from the turn point, then the number of inversions is given by,

$$N^{\text{after}} = \begin{cases} \left\lceil \left[ \frac{I_x + F_{\text{tp}}}{2K} \right] \right\rceil, & \text{if } \dot{t}_{\text{tp}} < 0, \\ \left\lceil \left[ \frac{I_x - F_{\text{tp}}}{2K} \right] \right\rceil + 1, & \text{if } \dot{t}_{\text{tp}} > 0, \end{cases} \quad (23)$$

where  $F_{\text{tp}}$  is the Incomplete Elliptic integral of first kind denoted as,

$$F_{\text{tp}} = F \left( \arccos \frac{t_{\text{tp}}}{t_+}, \frac{t_+^2}{t_-^2 + t_+^2} \right). \quad (24)$$

Note that, in Eq. (23), we distinguish the cases whether the function  $t(x)$  decreases or increases at the turn point. Note that, contrary to Eq. (19), we should take the limits of the  $I_x$ -integral for the particles moving from the turn point to infinity, e.g. in Eq. (23), as,

$$I_x = z \sqrt{t_+^2 + t_-^2} \int_{x_{\text{tp}}}^x \frac{dx'}{\sqrt{R(x')}}}, \quad (25)$$

where  $x_{\text{tp}} < x < \infty$ .

Using Eqs. (8) and (23), we can find  $\theta(x)$  for the outgoing neutrinos as,

$$\cos \theta_{\text{out}} = t_+ \times \begin{cases} \text{cn} \left( (-1)^{N^{\text{after}}} \left( I_x + F_{\text{tp}} - 4K \left[ \frac{N^{\text{after}}}{2} \right] \right) \middle| \frac{t_+^2}{t_-^2 + t_+^2} \right), & \text{if } \dot{t}_{\text{tp}} < 0, \\ \text{cn} \left( (-1)^{N^{\text{after}}} \left( F_{\text{tp}} - I_x + 4K \left[ \frac{N^{\text{after}}}{2} \right] \right) \middle| \frac{t_+^2}{t_-^2 + t_+^2} \right), & \text{if } \dot{t}_{\text{tp}} > 0. \end{cases} \quad (26)$$

where,  $\lceil \dots \rceil$  denotes the Ceiling function.

Similarly using Eqs. (9) and (23), we find  $\phi_{\text{out}}$  for an outgoing neutrino at the observer position as,

$$\phi_{\text{out}} = \begin{cases} z \int_{x_{\text{tp}}}^{\infty} \frac{(x - zy)dx}{(x^2 - x + z^2)\sqrt{R(x)}} + \frac{y}{zt_-} \left\{ 2N^{\text{after}}\Pi + \Pi_{\text{tp}} - (-1)^{N^{\text{after}}}\Pi_{t_{\text{obs}}} \right\}, & \text{if } \dot{t}_{\text{tp}} < 0, \\ z \int_{x_{\text{tp}}}^{\infty} \frac{(x - zy)dx}{(x^2 - x + z^2)\sqrt{R(x)}} + \frac{y}{zt_-} \left\{ 2N^{\text{after}}\Pi - \Pi_{\text{tp}} + (-1)^{N^{\text{after}}}\Pi_{t_{\text{obs}}} \right\}, & \text{if } \dot{t}_{\text{tp}} > 0. \end{cases} \quad (27)$$

Here,

$$t_{\text{obs}} = \cos \theta_{\text{obs}}, \quad \Pi_{t_{\text{obs}}} = \Pi \left( \arcsin(t_{\text{obs}}/t_+), t_+^2, -t_+^2/t_-^2 \right). \quad (28)$$

Note that  $\phi_{\text{obs}} = \phi_{\text{in}} + \phi_{\text{out}}$ . Moreover, since a neutrino can make multiple revolutions around the BH, this results in  $\phi_{\text{obs}}$  being greater than  $2\pi$ . One should account for it in the final analysis.

### B. Motion of the Lower Neutrinos

In a similar manner, we can also describe the trajectories of the Lower neutrinos. We write the expressions for all the relevant quantities in the following.

Before the turn point,

$$N^{\text{before}} = \left\lfloor \frac{I_x + F_i}{2K} \right\rfloor, \quad (29)$$

$$\cos \theta_{\text{in}} = t_+ \text{cn} \left( (-1)^{N^{\text{before}}} \left\{ F_i + I_x - 4K \left\lfloor \frac{N^{\text{before}}}{2} \right\rfloor \right\} \middle| \frac{t_+^2}{t_-^2 + t_+^2} \right), \quad (30)$$

$$\phi_{\text{in}} = z \int_{x_{\text{tp}}}^{\infty} \frac{(x - zy)dx}{(x^2 - x + z^2)\sqrt{R(x)}} + \frac{y}{zt_-} \left\{ 2N^{\text{before}}\Pi + \Pi_i - (-1)^{N^{\text{before}}}\Pi_{t_{\text{tp}}} \right\}, \quad (31)$$

After the turn point,

$$N^{\text{after}} = \begin{cases} \left\lfloor \frac{I_x + F_{\text{tp}}}{2K} \right\rfloor, & \text{if } \dot{t}_{\text{tp}} < 0, \\ \left\lfloor \frac{I_x - F_{\text{tp}}}{2K} \right\rfloor + 1, & \text{if } \dot{t}_{\text{tp}} > 0, \end{cases} \quad (32)$$

$$\cos \theta_{\text{out}} = t_+ \times \begin{cases} \text{cn} \left( (-1)^{N^{\text{after}}} \left( I_x + F_{\text{tp}} - 4K \left\lfloor \frac{N^{\text{after}}}{2} \right\rfloor \right) \middle| \frac{t_+^2}{t_-^2 + t_+^2} \right), & \text{if } \dot{t}_{\text{tp}} < 0, \\ \text{cn} \left( (-1)^{N^{\text{after}}} \left( F_{\text{tp}} - I_x + 4K \left\lfloor \frac{N^{\text{after}}}{2} \right\rfloor \right) \middle| \frac{t_+^2}{t_-^2 + t_+^2} \right), & \text{if } \dot{t}_{\text{tp}} > 0. \end{cases} \quad (33)$$

$$\phi_{\text{out}} = \begin{cases} z \int_{x_{\text{tp}}}^{\infty} \frac{(x - zy)dx}{(x^2 - x + z^2)\sqrt{R(x)}} + \frac{y}{zt_-} \left\{ 2N^{\text{after}}\Pi + \Pi_{t_{\text{tp}}} - (-1)^{N^{\text{after}}}\Pi_{t_{\text{obs}}} \right\}, & \text{if } \dot{t}_{\text{tp}} < 0, \\ z \int_{x_{\text{tp}}}^{\infty} \frac{(x - zy)dx}{(x^2 - x + z^2)\sqrt{R(x)}} + \frac{y}{zt_-} \left\{ 2N^{\text{after}}\Pi - \Pi_{t_{\text{tp}}} + (-1)^{N^{\text{after}}}\Pi_{t_{\text{obs}}} \right\}, & \text{if } \dot{t}_{\text{tp}} > 0. \end{cases} \quad (34)$$

Similar to the upper neutrinos,  $\phi_{\text{obs}} = \phi_{\text{in}} + \phi_{\text{out}}$  for the lower neutrinos too. Likewise since a neutrino can make multiple revolutions around the BH,  $\phi_{\text{obs}}$  can be greater than  $2\pi$ . One should adjust it in the final analysis.

In Figs. 3(a) and 3(b), we plot  $\cos \theta$  versus  $r$  for the trajectories of a few upper and lower neutrinos for  $a = 0.02M$  and  $a = 0.98M$ , respectively. The neutrinos are moving in the pure gravitational field of the BH. We see that the  $\cos \theta$  of the neutrinos change signs near the turn point implying crossing of neutrinos from above the equatorial plane to below and vice versa.

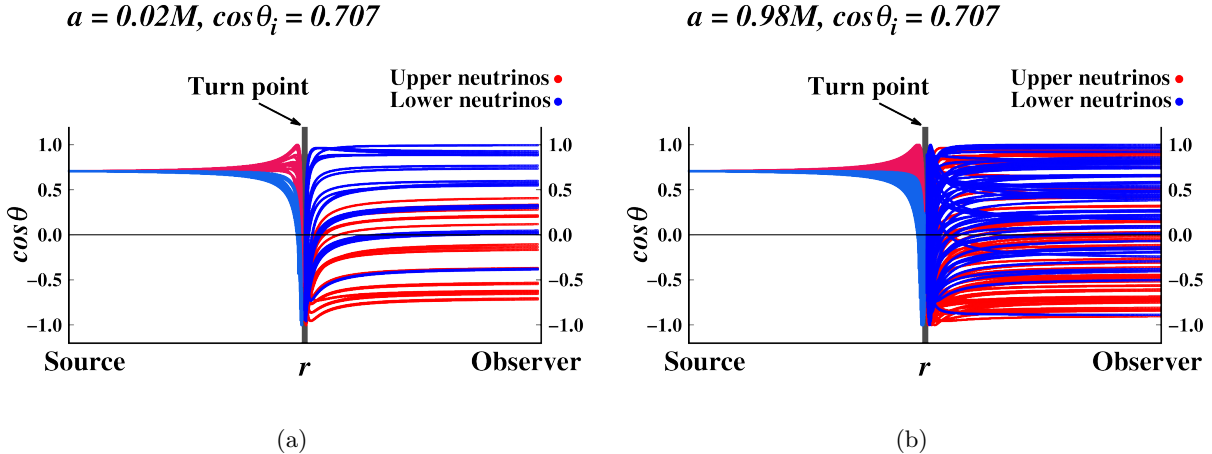


FIG. 3. Figures showing  $r$  vs  $\cos \theta$  for the trajectories of a few upper and lower neutrinos. We see that they experience change in signs in  $\cos \theta$ . This implies crossing of neutrinos from above the equatorial plane to below and vice versa. (a)  $a = 0.02M$  and (b)  $a = 0.98M$ .

#### IV. NEUTRINO SPIN EVOLUTION IN CURVED SPACE-TIME

In Sec. III, we define the neutrino trajectories. As mentioned earlier, a neutrino interacts electroweakly with the accretion disk besides gravity. In addition, it experiences spin precession due to the electromagnetic interaction with the magnetized disk [28]. In this section, we shall discuss the neutrino spin evolution along these trajectories.

It is well known that the spin evolution of an elementary fermion of mass  $m$  in flat space-time obeys the Bargmann-Michel-Telegdi (BMT) equation [32] as,

$$\frac{dS^\mu}{d\tau} = 2\mu F^{\mu\nu} S_\nu - 2\mu' u^\mu F^{\nu\lambda} u_\nu S_\lambda, \quad (35)$$

where  $F_{\mu\nu}$  is the electromagnetic field tensor, and  $\tau$  is the proper time. The quantities,  $\mu$  and  $\mu' = \mu - \mu_B$ , are the magnetic and anomalous magnetic moments, respectively, while  $\mu_B = \frac{e}{2m} = 5.8 \times 10^{-9} \text{ eV} \cdot \text{G}^{-1}$  is the Bohr magneton.  $u^\mu = \frac{dx^\mu}{d\tau} = p^\mu/m$  is the particle four velocity which satisfies the Lorentz equation,

$$m \frac{du^\mu}{d\tau} = eF^{\mu\nu} u_\nu. \quad (36)$$

Since a neutrino is an electrically neutral particle, hence  $\mu = \mu'$  i.e. the magnetic moment is purely anomalous. Moreover,  $\frac{du^\mu}{d\tau} = 0$  in Eq. (36), i.e. a neutrino moves along a straight line in the flat space-time.

Equation (35) is then generalized to include the electroweak interactions of neutrinos with the

background matter in Ref. [33] as follows,

$$\frac{dS^\mu}{d\tau} = 2\mu(F^{\mu\nu}S_\nu - u^\mu F^{\nu\lambda}u_\nu S_\lambda) + \sqrt{2}G_F\varepsilon^{\mu\nu\lambda\rho}G_\nu u_\lambda S_\rho, \quad (37)$$

where  $\varepsilon^{\mu\nu\lambda\rho}$  is the antisymmetric tensor in Minkowski space-time with the signature  $\varepsilon^{0123} = 1$ , and  $G_F = 1.17 \times 10^{-5} \text{ GeV}^{-2}$  is the Fermi constant. The quantity,  $G^\mu$ , is the contravariant effective potential for the neutrino electroweak interactions with a background matter defined as,

$$G^\mu = \sum_f \left( q_f^{(1)} j_f^\mu + q_f^{(2)} \lambda_f^\mu \right). \quad (38)$$

Here,  $j_f^\mu$  is the hydrodynamic current of background fermions of the type  $f$ ,  $\lambda_f^\mu$  is their polarization. The constants,  $q_f^{(1,2)}$ , are given in Ref. [33] for different oscillation channels.

If we now consider a spinning particle in curved spacetime, the evolution of the particle's four momentum in an external gravitational field is given in Refs. [6, 34]

$$\frac{Dp^\mu}{d\tau} = -\frac{1}{2}R^\mu_{\nu\rho\lambda}u^\nu S^{\rho\lambda}, \quad (39)$$

where  $R^\mu_{\nu\rho\lambda}$  is the Riemann tensor. The spin-tensor  $S_{\mu\nu}$  is related to the spin four vector by

$$S^\mu = -\frac{1}{m^2}E^{\mu\nu\lambda\rho}p_\nu S_{\lambda\rho}, \quad (40)$$

where  $E^{\mu\nu\lambda\rho} = \frac{\varepsilon^{\mu\nu\lambda\rho}}{\sqrt{-g}}$  is the antisymmetric tensor in the curved space-time,  $g = \det(g_{\mu\nu})$  for the given metric  $g_{\mu\nu}$ , and  $m$  is the particle mass which is the integral of motion:  $m^2 = p^2$ . It is clear from Eq. (40) that  $Dp^\mu \neq 0$  if  $R^\mu_{\nu\rho\lambda} \neq 0$ . Moreover, the four velocity  $u^\mu$  and the particle four momentum  $p^\mu$  are not collinear in the general situation. Thus, unlike in the case of flat space-time, the motion of a neutrino deviates from the geodesics in an external gravitational field. However, in deriving of Eq. (39) in, e.g. Refs. [6, 34], one assumes that the size of the spinning body is finite. In the case of an elementary point-like particle, it is mentioned in Refs. [6, 34] that it moves along a geodesic.

Based on this fact, the formalism where the spin, e.g. of a neutrino, is parallel transported along the geodesics is proposed in Ref. [35]. These results are later confirmed in the works of Refs. [36, 37] which use the quantum approach based on the Dirac equation analysis in curved space-time.

Finally the spin evolution of neutrinos along the geodesics is given in Ref. [9] by generalizing the Eq. (37) in curved space-time as,

$$\frac{DS^\mu}{d\tau} = 2\mu(F^{\mu\nu}S_\nu - U^\mu F^{\nu\lambda}U_\nu S_\lambda) + \sqrt{2}G_F E^{\mu\nu\lambda\rho}G_\nu U_\lambda S_\rho. \quad (41)$$

The definition of  $G^\mu$  remains the same as in Eq. (38),  $j_f^\mu = n_f U_f^\mu$ , where  $n_f$  is the invariant number density of background fermions, and  $U_f^\mu$  is the their four velocity in the curved space-time.

Instead of dealing with the Eq. (41) in curved space-time, it is rather convenient to reformulate it for the invariant 3D spin vector. For this purpose, we first make a transformation to a locally Minkowskian frame,  $x_a = e_a^\mu x_\mu$ , where  $e_a^\mu$  ( $a = 0 \cdots 3$ ) are the vierbein vectors satisfying the relations,

$$e_a^\mu e_b^\nu g_{\mu\nu} = \eta_{ab}, \quad e_\mu^a e_\nu^b \eta_{ab} = g_{\mu\nu}. \quad (42)$$

Here,  $\eta_{ab} = \text{diag}(1, -1, -1, -1)$ , is the Minkowski metric tensor. For the Kerr metric in Eq. (1), the explicit form of the vierbein vectors can be written as,

$$\begin{aligned} e_0^\mu &= \left( \sqrt{\frac{\Xi}{\Sigma\Delta}}, 0, 0, \frac{arrg}{\sqrt{\Sigma\Delta\Xi}} \right), \quad e_1^\mu = \left( 0, \sqrt{\frac{\Delta}{\Sigma}}, 0, 0 \right), \\ e_2^\mu &= \left( 0, 0, \frac{1}{\sqrt{\Sigma}}, 0 \right), \quad e_3^\mu = \left( 0, 0, 0, \frac{1}{\sin\theta} \sqrt{\frac{\Sigma}{\Xi}} \right), \end{aligned} \quad (43)$$

where  $\Sigma$ ,  $\Delta$  and  $\Xi$  are given in Eq. (2).

If we now make a boost to the particle rest frame, we can write the polarization of a neutrino in terms of an invariant three vector  $\zeta$ . The evolution of the neutrino polarization vector obeys,

$$\frac{d\zeta}{dt} = 2(\zeta \times \Omega), \quad (44)$$

where,

$$\Omega = \Omega^g + \Omega^{\text{em}} + \Omega^{\text{matt}}. \quad (45)$$

The gravitational, electromagnetic and electroweak interactions,  $\Omega^{\text{g,em,matt}}$ , respectively, are given in Refs. [17, 18] as,

$$\begin{aligned} \Omega^g &= \frac{1}{2Ut} \left[ \mathbf{b}_g + \frac{1}{1+u^0} (\mathbf{e}_g \times \mathbf{u}) \right], \\ \Omega^{\text{em}} &= \frac{\mu}{Ut} \left[ u^0 \mathbf{b} - \frac{\mathbf{u}(\mathbf{u}\mathbf{b})}{1+u^0} + (\mathbf{e} \times \mathbf{u}) \right], \\ \Omega^{\text{matt}} &= \frac{G_F \mathbf{u}}{\sqrt{2}Ut} \left( g^0 - \frac{(\mathbf{g}\mathbf{u})}{1+u^0} \right). \end{aligned} \quad (46)$$

Here  $u^a = (u^0, \mathbf{u}) = e^a_\mu U^\mu$  are velocity vectors with respect to the locally Minkowskian frame,  $U^\mu = \frac{dx^\mu}{d\tau}$  is the particle velocity in world coordinates,  $G_{ab} = (\mathbf{e}_g, \mathbf{b}_g) = \gamma_{abc} u^c$ ,  $\gamma_{abc} = \eta_{ad} e^d_{\mu;\nu} e_b^\mu e_c^\nu$  are the Ricci rotation coefficients. The semicolon stands for covariant derivative. Moreover,  $f_{ab} = e_a^\mu e_b^\nu F_{\mu\nu} = (\mathbf{e}, \mathbf{b})$  is the electromagnetic field tensor in the locally Minkowskian frame, and  $g^a = (g^0, \mathbf{g}) = e^a_\mu G^\mu$ .

In terms of the dimensionless variables, the quantities,  $\Omega_x^{\text{g,em,matt}}$ , take the form as,

$$\Omega_x^{\text{g}} = \frac{1}{2} \left[ \tilde{\mathbf{b}}_g + (\tilde{\mathbf{e}}_g \times \mathbf{v}) \right], \quad (47)$$

$$\Omega_x^{\text{em}} = V_B \left[ l^0 \mathbf{b} - \mathbf{v}(l\mathbf{b}) + (\mathbf{e} \times l) \right], \quad (48)$$

$$\Omega_x^{\text{matt}} = V_m l \left[ g^0 - (\mathbf{g}\mathbf{v}) \right], \quad (49)$$

where the vectors,  $(l^0, \mathbf{l}) = l^a = \frac{dt}{dr} \frac{u^a}{U^t}$ ,  $\mathbf{v} = \frac{\mathbf{u}}{1+u^0}$ ,  $\tilde{\mathbf{e}}_g = \mathbf{e}_g \frac{r_g}{U^t} \frac{dt}{dr}$  and  $\tilde{\mathbf{b}}_g = \mathbf{b}_g \frac{r_g}{U^t} \frac{dt}{dr}$ , are finite for an ultra-relativistic neutrino. Their explicit expressions are given in Appendix B. The coefficients are  $V_m = \frac{G_F}{\sqrt{2}m_p r_g^3}$  and  $V_B = \left(\frac{\mu}{r_g}\right)^2$ , as well as  $m_p$  is the mass of proton.

However instead of the precession Eq. (44), it is numerically more convenient to study the effective Schrödinger equation for the description of the neutrino polarization,

$$i \frac{d\psi}{dx} = \hat{H}_x \psi, \quad (50)$$

where,

$$\hat{H}_x = -\mathcal{U}_2 (\boldsymbol{\sigma} \cdot \boldsymbol{\Omega}_x) \mathcal{U}_2^\dagger, \quad \boldsymbol{\Omega}_x = r_g \boldsymbol{\Omega} \frac{dt}{dr}, \quad \mathcal{U}_2 = \exp(i\pi\sigma_2/4). \quad (51)$$

Here  $\boldsymbol{\sigma} = (\sigma_1, \sigma_2, \sigma_3)$  are the Pauli matrices. The Hamiltonian  $\hat{H}_x$  is the function of  $x$  only through the dependence of  $\theta(x)$  given in Eqs. (20), (26), (30) and (33).

We solve the Eq. (50) numerically at every  $x$  separately for the upper and lower neutrinos. Since we consider that all incoming neutrinos are left polarized at the infinity traveling at angle  $\theta_i$  with respect to the equatorial plane of the BH, the initial condition can be written in the form,  $\psi_{-\infty}^T = (1, 0)$ . We use discrete grid for the motion of the neutrinos. Our grid is also irregular having denser points gradually towards the BH. We first use 4th order Adam-Bashforth predictor method for an irregular grid to obtain the (approximate) solutions at  $x$ . However as a neutrino approaches the BH, there is a probability that we deal with a Stiff equation. In order to avoid numerically unstable solutions, we then use Adam-Moulton corrector method to iteratively improve the solutions obtained from the Adam-Bashforth method with appropriate convergence conditions. The details of the 4th order Adam-Bashforth and Adam-Moulton methods are provided in Appendix C.

There are two convergence condition that we use in the Adam-Moulton method. The first one deals with the convergence of each of the 4 components of  $\psi(x)$ , and the second one checks whether the normalization condition is satisfied within a particular iteration. In our case, these two conditions can be written as,

$$\left| \frac{\psi^j(x)_k - \psi^j(x)_{k-1}}{\psi^j(x)_{k-1}} \right| \leq 10^{-15}, \quad |\psi(x)_k|^2 = 1 \pm O(10^{-15}), \quad (52)$$

where,  $k$  is the iteration number in the determination of the  $j$ -th component of  $\psi(x)$ . When both the conditions are satisfied, the solution is accepted.

After finding  $\psi_{+\infty}^T = (\psi_{+\infty}^{(R)}, \psi_{+\infty}^{(L)})$  numerically, we then compute  $P_{LL} = |\psi_{+\infty}^{(L)}|^2$  at the observer position. Here, we take into account that the neutrino velocity changes its direction in the locally Minkowskian frame after the scattering. The angular co-ordinate  $\theta_{\text{obs}}$  can be computed from Eqs. (26) and (33). Similarly,  $\phi_{\text{obs}}$  can be computed from Eqs. (21), (27), (31) and (34).

## V. “POLISH DOUGHNUT” MODEL OF MAGNETIZED ACCRETION DISK

There exists several models of accretion disk surrounding a black hole (For a review, see e.g. Ref. [38]). For our study, when a neutrino crosses the disk, its path should be long enough for the spin to rotate on a sizable angle with respect to the neutrino velocity. For this reason, we adopt a thick “Polish doughnut” disk proposed in Ref. [27]. This model is later generalized in Ref. [28] to accommodate for the toroidal magnetic field.

The plasma motion in an accretion disk is quite complex. We assume that the hydrogen plasma is unpolarized, and we treat the electroweak interaction of a neutrino with the fermions in the plasma in the forward scattering approximation. We admit that the accretion disk can rotate around BH with relativistic velocities. We also assume that the plasma is electrically neutral, i.e. the invariant number density of electrons and protons are equal,  $n_e = n_p$ . The four potential,  $G^\mu$ , for the neutrino electroweak interactions with a background matter can then be written as,

$$G^\mu = \sum_{f=e,p} q_f J_f^\mu, \quad (53)$$

where  $J_f^\mu = n_f U_f^\mu$  are the hydrodynamic currents, and  $U_f^\mu$  are the four velocities of fermions in the disk. We assume that  $U_e^\mu = U_p^\mu$ , i.e. there is no differential rotation between the components of the plasma.

The only non-zero components in Eq. (53) are  $J_f^t = n_f U_f^t \neq 0$  and  $J_f^\phi = n_f U_f^\phi \neq 0$  because of the axial symmetry of the disk. Then the four potential in the locally Minkowskian frame,  $g^a = e^a_\mu G^\mu$  can be written as,

$$g^a = (g^0, 0, 0, g^3). \quad (54)$$

The explicit forms of  $g^0$  and  $g^3$  are provided in Appendix B.

We can define the invariant extensions for the electric and magnetic fields in the plasma as,

$$E_\mu = F_{\mu\nu} U_f^\nu, \quad B_\mu = \tilde{F}_{\mu\nu} U_f^\nu, \quad \tilde{F}_{\mu\nu} = \frac{1}{2} E_{\mu\nu\alpha\beta} F^{\alpha\beta}. \quad (55)$$

Since the plasma is electrically neutral,  $E_\mu = 0$ . If we choose  $U_f^\mu = (U_f^t, 0, 0, U_f^\phi)$  and  $B^\mu = (B^t, 0, 0, B^\phi)$ , then all the parameters of the disk depend on  $r$  and  $\theta$  due to the axial symmetry of the metric in eq. (1). Then the only non-zero component of the electromagnetic field tensor  $F^{r\theta} = -F^{\theta r}$ . In that case, only the  $b_3$  component of the toroidal magnetic field in the local Minkowskian frame becomes non-zero. The explicit form of  $b_3$  is given in Appendix B.

We further assume that the specific angular momentum of a particle in the disk  $l = L/E$  is constant,  $l = l_0$ . Here  $E = mU_f^t$  is the energy of the particle,  $L = -mU_f^\phi$  is its angular momentum, and  $m$  is its mass.

Following Refs. [27, 28], if we define the generating function for the disk potential as,

$$W(r, \theta) = \frac{1}{2} \ln \left| \frac{\mathcal{L}}{\mathcal{A}} \right|, \quad (56)$$

then disk density  $\rho$  and the magnetic pressure  $p_m^{(\text{tor})}$  can be written as,

$$\rho = \left[ \frac{\kappa - 1}{\kappa} \frac{W_{\text{in}} - W}{K + K_m \mathcal{L}^{\kappa-1}} \right]^{\frac{1}{\kappa-1}}, \quad p_m^{(\text{tor})} = K_m \mathcal{L}^{\kappa-1} \left[ \frac{\kappa - 1}{\kappa} \frac{W_{\text{in}} - W}{K + K_m \mathcal{L}^{\kappa-1}} \right]^{\frac{\kappa}{\kappa-1}}, \quad (57)$$

where  $K$ ,  $K_m$ , and  $\kappa$  are the constants in the equations of state. We choose  $\kappa = 4/3$  as in Ref. [28].

The parameter  $W_{\text{in}}$  in eq. (57) is the value of  $W$  at the border of the disk. The maximal effective toroidal field is given by  $|\mathbf{B}|_{\text{max}}^{(\text{tor})} = \sqrt{2p_m^{(\text{tor})}}$ .

The components of  $U_f^\mu$  and  $B^\mu$  can then be written as,

$$U_f^t = \sqrt{\left| \frac{\mathcal{A}}{\mathcal{L}} \right|} \frac{1}{1 - l_0 \Omega}, \quad U_f^\phi = \Omega U_f^t, \quad (58)$$

$$B^\phi = \sqrt{\frac{2p_m^{(\text{tor})}}{|\mathcal{A}|}}, \quad B^t = l_0 B^\phi, \quad (59)$$

where,

$$\mathcal{L} = g_{tt} g_{\phi\phi} - g_{t\phi}^2, \quad (60)$$

$$\mathcal{A} = g_{\phi\phi} + 2l_0 g_{t\phi} + l_0^2 g_{tt}, \quad (61)$$

$$\Omega = -\frac{g_{t\phi} + l_0 g_{tt}}{g_{\phi\phi} + l_0 g_{t\phi}}. \quad (62)$$

Here,  $\Omega$  is the angular velocity in the disk.

Equations (56)-(62) completely define all the characteristics of the disk. For computation, we use the dimensionless variables  $\tilde{K} = r_g^{4(1-\kappa)} K$  and  $\tilde{K}_m = r_g^{2(1-\kappa)} K_m$ . The methods to determine the values of  $\tilde{K}$ ,  $\tilde{K}_m$ ,  $\rho$ , and  $p_m^{(\text{tor})}$  are discussed in Sec. VI

Note that the explicit value of the specific angular momentum,  $l_0$ , depends on whether the disk is co-rotating or counter-rotating [39]. The Keplerian angular momentum in terms of the dimensionless variable is given by [18, 28],

$$l(x) = \frac{\pm(x^2 \mp z\sqrt{2x} + z^2)}{\sqrt{2}x^{3/2} - \sqrt{2x} \pm z}. \quad (63)$$

where the upper sign is used for a co-rotating disk and the lower sign for a counter-rotating one. Using Eq. (63), one can define two quantities  $l_{\text{mb}}$  and  $l_{\text{ms}}$  which are the functions of the dimensionless radii of the marginally bound Keplerian orbits,  $x_{\text{mb}}$ , and, marginally stable Keplerian orbits,  $x_{\text{ms}}$ , respectively. The values of  $x_{\text{mb}}$  and  $x_{\text{ms}}$  also depend on whether the disk is co-rotating or counter-rotating, and one shall compute them accordingly [39]. They are given as,

$$x_{\text{mb}} = 1 \mp z + \sqrt{1 \mp 2z}, \quad (64)$$

$$x_{\text{ms}} = \frac{1}{2}[3 + Z_2 \mp \sqrt{(3 - Z_1)(3 + Z_1 + 2Z_2)}], \quad (65)$$

where,

$$Z_1 = 1 + (1 - 4z^2)^{1/3}[(1 + 2z)^{1/3} + (1 - 2z)^{1/3}], \quad (66)$$

$$Z_2 = \sqrt{12z^2 + Z_1^2}. \quad (67)$$

We then take the value of  $l_0$  as,

$$l_0 = 0.6(l_{\text{mb}} + l_{\text{ms}}). \quad (68)$$

In our current work, we consider both co-rotating or counter-rotating disks.

TABLE I. The values of the parameters that are common to various combinations of BH spins and incident angles.

BH mass	$\mu$	$W_{\text{in}}$	$n_e^{\text{max}}$	$ \mathbf{B} _{\text{max}}^{(\text{tor})}$	$r_g$	$V_{\text{B}}$	$V_m$
$10^8 M_{\odot}$	$10^{-13} \mu_{\text{B}}$	$10^{-5}$	$10^{18} \text{ cm}^{-3}$	320 G	$3 \times 10^{13} \text{ cm}$	$4 \times 10^{-76}$	$2.5 \times 10^{-87}$

## VI. NUMERICAL METHODS AND PARAMETERS

In our study, we fix the mass of SMBH at  $M = 10^8 M_{\odot}$ . We consider three different spins of SMBH, e.g.  $a = 2 \times 10^{-2} M, 0.50M$  and  $0.98M$ . For each BH spin, we consider eight different

TABLE II. The values of  $\tilde{K}$  and  $\tilde{K}_m$  for different BH spins for both the co-rotating and counter-rotating disks.

Disk type	BH Spin	$\tilde{K}$	$\tilde{K}_m$
Co-rotating	$a = 0.02M$	$2.55 \times 10^{-31}$	$3.59 \times 10^{-41}$
	$a = 0.50M$	$2.87 \times 10^{-31}$	$3.01 \times 10^{-41}$
	$a = 0.98M$	$9.35 \times 10^{-31}$	$9.86 \times 10^{-41}$
Counter-rotating	$a = 0.02M$	$2.44 \times 10^{-31}$	$3.62 \times 10^{-41}$
	$a = 0.50M$	$1.96 \times 10^{-31}$	$3.12 \times 10^{-41}$
	$a = 0.98M$	$1.66 \times 10^{-31}$	$2.71 \times 10^{-41}$

TABLE III. Number of gravitationally scattered neutrinos (in million) used for various combinations of BH spins and angles of incidence. The numbers for both the co-rotating and counter-rotating disks are listed.

Disk type	BH Spin	Number of Neutrinos ( $\times 10^6$ ) at $\cos \theta_i =$							
		0.01	-0.01	0.50	-0.50	0.707	-0.707	0.90	-0.90
Co-rotating	$a = 0.02M$	2.68	2.68	3.20	3.20	2.32	2.32	2.68	2.68
	$a = 0.50M$	2.78	2.78	3.45	3.45	2.56	2.56	2.97	2.97
	$a = 0.98M$	2.91	2.91	4.04	4.00	3.24	3.25	3.99	4.00
Counter-rotating	$a = 0.02M$	2.69	2.69	3.20	3.20	2.33	2.33	2.68	2.68
	$a = 0.50M$	2.78	2.78	3.45	3.37	2.56	2.56	2.97	2.97
	$a = 0.98M$	3.32	3.32	4.83	4.83	3.75	3.75	4.21	4.21

incident angles,  $\cos \theta_i = \pm 0.01, \pm 0.50, \pm 0.707$  and  $\pm 0.90$ . We adopt a thick ‘‘Polish doughnut’’ model for the accretion disk [27]. The accretion disk consists of hydrogen plasma. We consider both co-rotating and counter-rotating disks around the SMBH with a relativistic velocity [28].

The magnetic moment of the Dirac neutrinos is taken to be  $\mu = 10^{-13} \mu_B$  where  $\mu_B$  is the Bohr magneton. This value is less than the astrophysical upper bound of the magnetic moment [40]. We assume that the neutrinos undergo electroweak interaction with the plasma of the accretion disk in the forward scattering approximation [33]. We also assume the neutrino spin oscillations within one neutrino generation, i.e. we suppose that only the diagonal magnetic moment is present.

We set the value of the generating function,  $W$ , at the inner border of the disk,  $W_{\text{in}} = 10^{-5}$ . The values of the parameters that are common to various BH spins and incident angles are listed in

Table I.

In order to determine the parameters  $\tilde{K}$  and  $\tilde{K}_m$ , we first choose the maximal number density of electrons to be  $n_e^{\max} = 10^{18} \text{ cm}^{-3}$  [41] such that the normalized electron number density distributions is  $n_e/10^{18} \text{ cm}^{-3}$ , where  $n_e = \rho/m_p$ ,  $m_p$  being the mass of proton. This provides us the value of  $\rho^{\max}$ . For the maximal strength of the toroidal field, we set it to be at  $|\mathbf{B}|_{\max}^{(\text{tor})} = 320 \text{ G}$ . This is  $\sim 1\%$  of the Eddington limit for this type of SMBH [42]. Using Eq. (57), we simultaneously vary  $\tilde{K}$  and  $\tilde{K}_m$  to match to  $\rho^{\max}$  and  $|\mathbf{B}|_{\max}^{(\text{tor})} = \sqrt{2\rho_m^{(\text{tor})}}$  for each spin of BH. Note that the value of the generating function,  $W$ , also depends whether the disk is co-rotating or counter-rotating. Therefore, one has to find the values of  $\tilde{K}$  and  $\tilde{K}_m$  for both the co-rotating and counter-rotating disks for each BH spin. The distributions of the electron number density and effective toroidal field,  $|\mathbf{B}|^{(\text{tor})}$ , for both the co-rotating and counter-rotating disks are shown in Figs. 4 and 5. The values of  $\tilde{K}$  and  $\tilde{K}_m$  are listed in Table II.

For our numerical work, we use more than 288 cores of IceLake and 1920 SkyLake processors in Govorun super-cluster at the Joint Institute for Nuclear Research. The number of gravitationally scattered neutrinos we use for each combination of BH spin and incident angle is more than 2 million. The detailed numbers are listed in Table III.

Here we would like to emphasize that unlike in the previous studies [15–19] where MATLAB based codes were used, the numerical studies for this work are based on a freshly written C++ code which is more efficient, optimized and flexible. Although it closely follow the old MATLAB code, it is a totally independent code. In the process rewriting the code in C++, we have realized a significant incorrectness in the results produced by the old MATLAB code when we considered only toroidal field in the accretion disk. The values of two dimensionless coefficients in Eqs. (48) and (49),  $V_B \sim O(10^{-76})$  and  $V_m \sim O(10^{-87})$  (e.g. see Ref [18]), respectively, turn out to be quite low for MATLAB's default precision. As a result, the MATLAB code produced the numerical values of plasma density and magnetic pressure to be zero's. In such a situation, the effect spin precession is not visible if we consider toroidal magnetic field only. This issue is ratified in [43] as well as in this work, and we present our new results by considering only toroidal field in the accretion disk.

## VII. RESULTS AND DISCUSSION

In this study, we consider three BH spins, namely  $a = 2 \times 10^{-2}M, 0.50M$  and  $0.98M$ . For each BH spin, we consider eight different incident angles,  $\cos \theta_i = \pm 0.01, \pm 0.50, \pm 0.707$  and  $\pm 0.90$ . For each combination of BH spin and incident angle, we consider more than 2 million neutrinos as

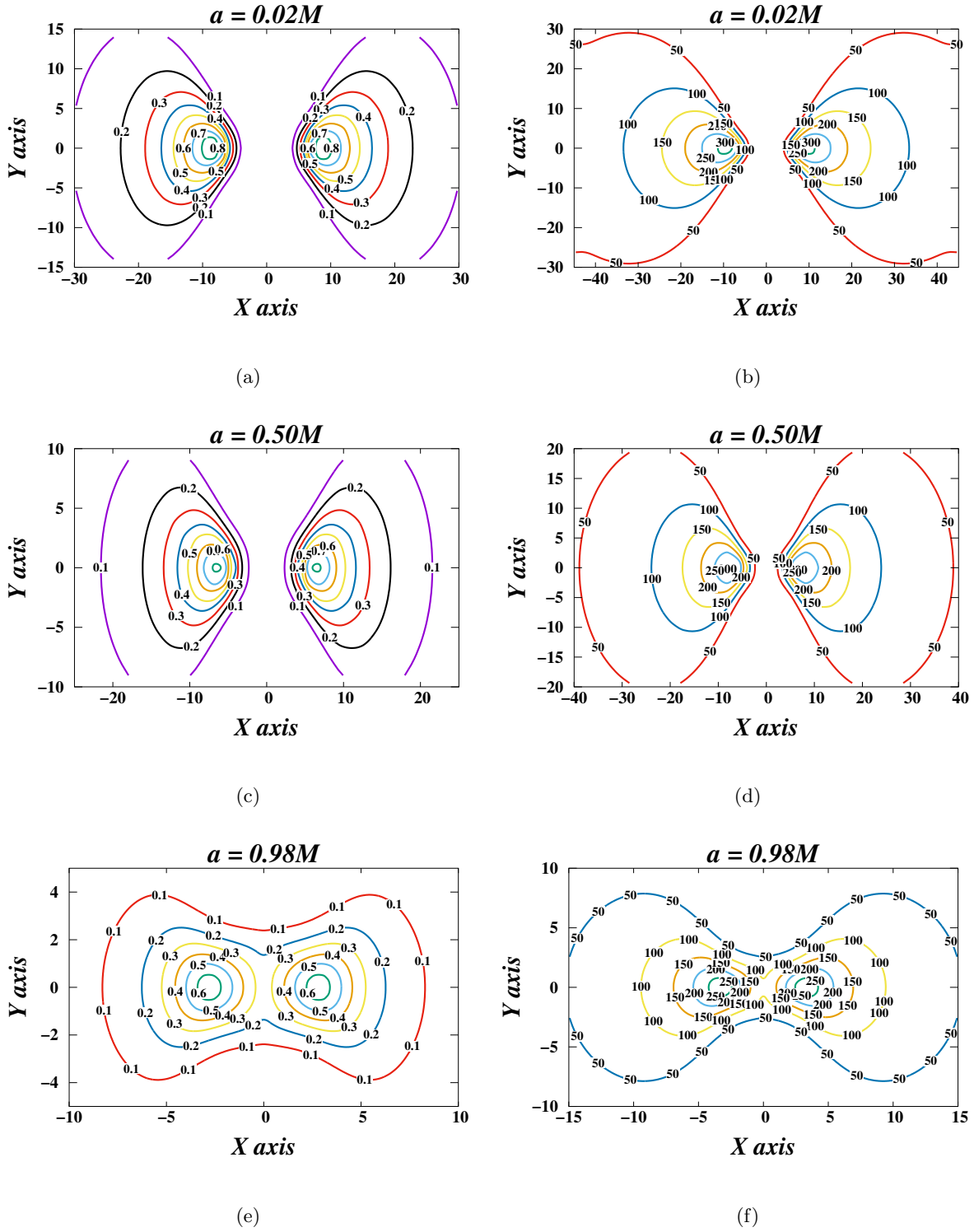


FIG. 4. Distribution profiles for the co-rotating disk. (a), (c) and (e): The distributions of the normalized electron number density,  $n_e/10^{18} \text{ cm}^{-3}$  for the BH spin  $a = 2 \times 10^{-2}M, 0.50M$  and  $0.98M$ , respectively. (b), (d), (e): The distributions of the effective toroidal magnetic field,  $|\mathbf{B}|^{(\text{tor})}$ , for the BH spin  $a = 2 \times 10^{-2}M, 0.50M$  and  $0.98M$ , respectively. The distances in the horizontal and vertical axes are in units of  $r_g$ .

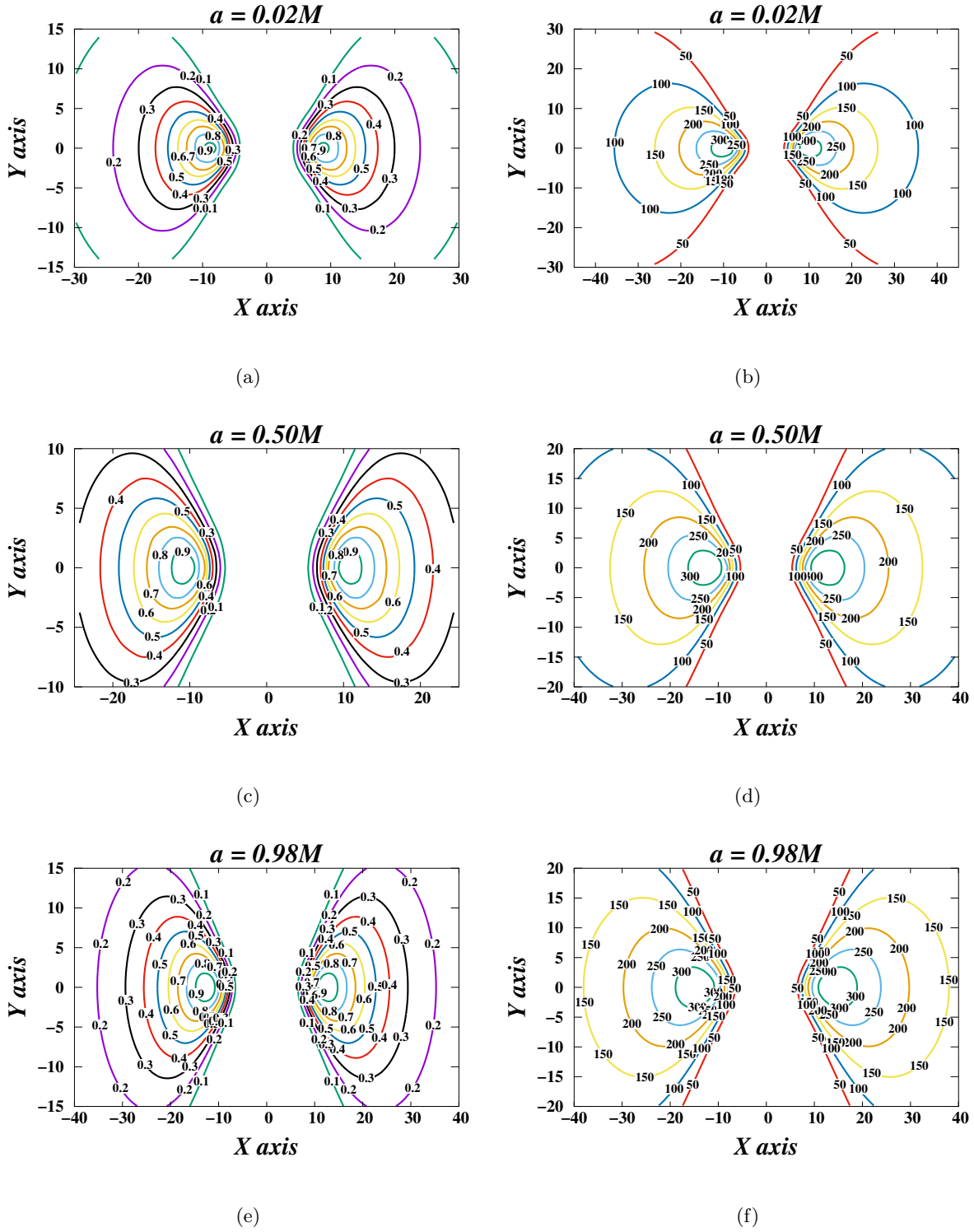


FIG. 5. Distribution profiles for the counter-rotating disk. (a), (c) and (e): The distributions of the normalized electron number density,  $n_e/10^{18} \text{ cm}^{-3}$  for the BH spin  $a = 2 \times 10^{-2}M, 0.50M$  and  $0.98M$ , respectively. (b), (d), (e): The distributions of the effective toroidal magnetic field,  $|\mathbf{B}|^{(\text{tor})}$ , for the BH spin  $a = 2 \times 10^{-2}M, 0.50M$  and  $0.98M$ , respectively. The distances in the horizontal and vertical axes are in units of  $r_g$ .

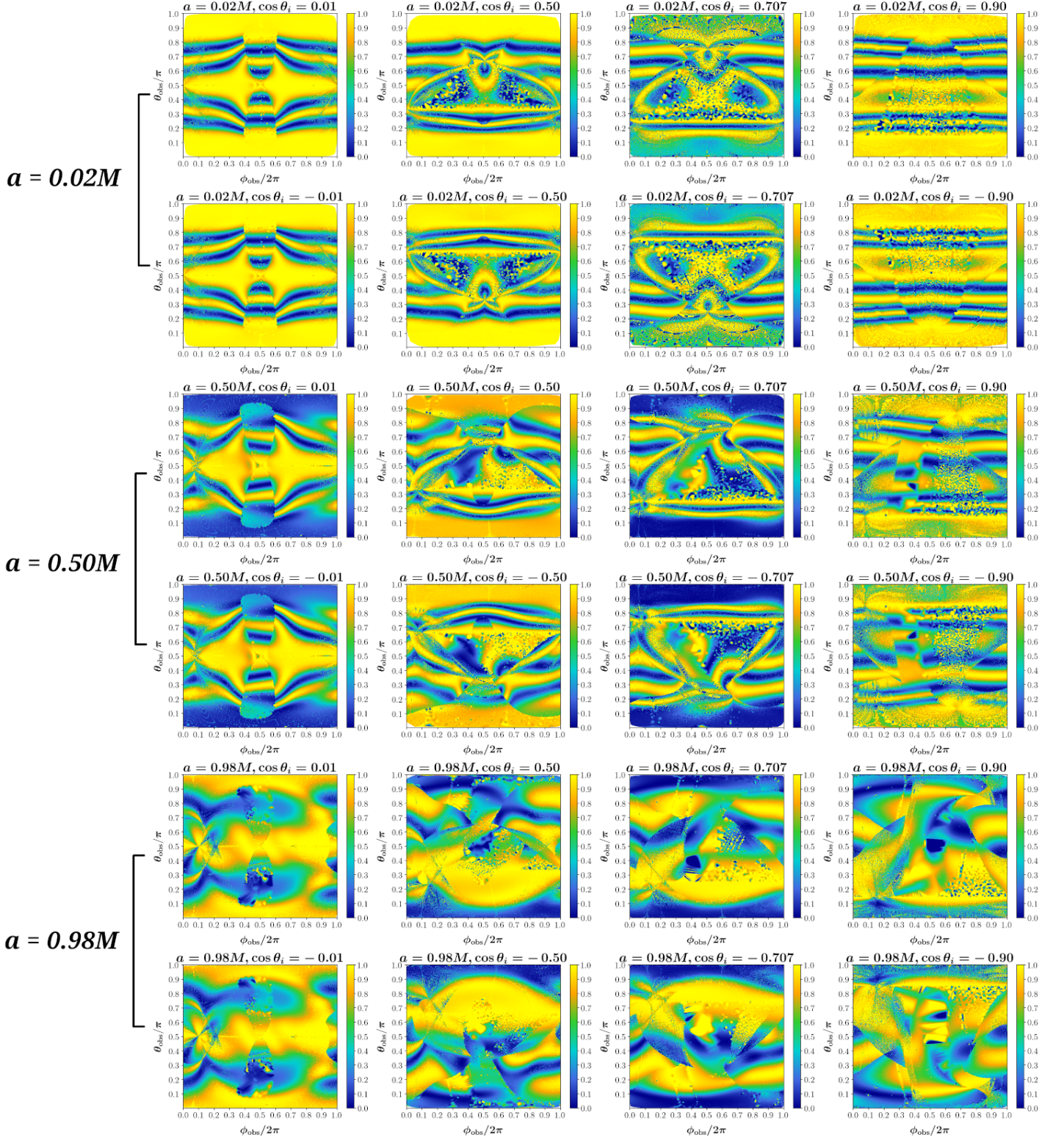


FIG. 6. The distributions of the survival probability,  $P_{LL}$  at  $(\theta_{\text{obs}}, \phi_{\text{obs}})$  for the co-rotating accretion disks. Figures show three BH spins  $a = 2 \times 10^{-2}M, 0.50M$  and  $0.98M$  and eight incident angles,  $\cos \theta_i = \pm 0.01, \pm 0.50, \pm 0.707$  and  $\pm 0.90$ .

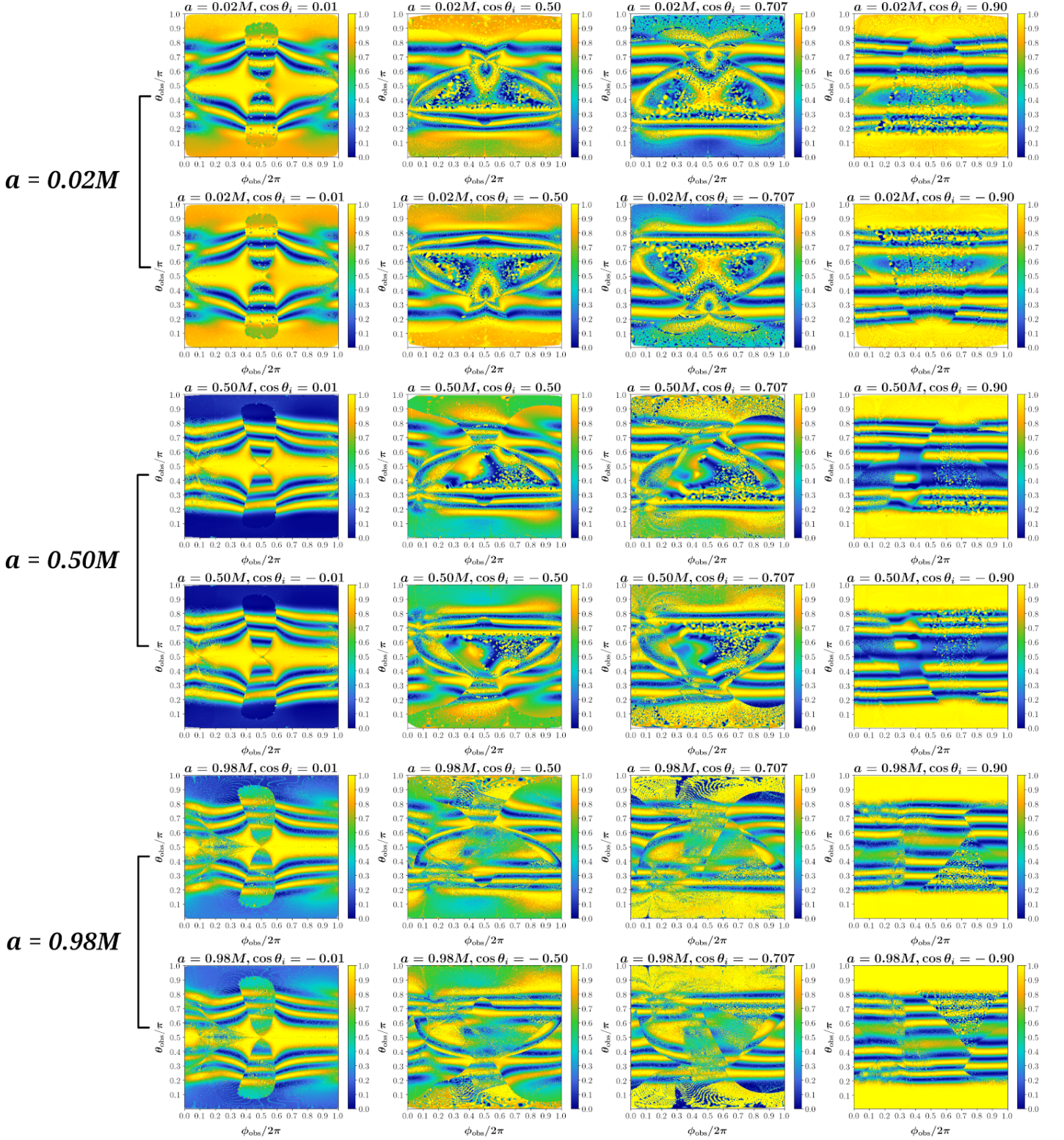


FIG. 7. The distributions of the survival probability,  $P_{\text{LL}}$  at  $(\theta_{\text{obs}}, \phi_{\text{obs}})$  for the counter-rotating accretion disks. Figures show three BH spins  $a = 2 \times 10^{-2}M, 0.50M$  and  $0.98M$  and eight incident angles,  $\cos \theta_i = \pm 0.01, \pm 0.50, \pm 0.707$  and  $\pm 0.90$ .

shown in the Table III.

If the spin of a left-handed Dirac neutrino precesses in an external field, it becomes sterile or right-handed. Such a neutrino cannot be observed in a detector. Hence, the observed flux of neutrinos will be reduced by a factor of  $P_{LL}$  in comparison to the flux of non-spinning particles.

We present our results for the co-rotating disk in Fig. 6 and for the counter-rotating disk in Fig. 7 as functions of  $\theta_{\text{obs}}$  and  $\phi_{\text{obs}}$ . The angles at which the incoming neutrinos are incident are mentioned above. Also as mentioned earlier, we consider only toroidal magnetic field in the accretion disk. All the areas with  $P_{LL} < 1$  signify spin flip of neutrinos. Lower the value of  $P_{LL}$ , the higher is the probability of the spin flip. We see that in all cases in Figs. 6 and 7, there are non-negligible probabilities of spin flip.

The result we obtain is different from what is reported in the studies [15–19]. In particular, we find that a sizable neutrino spin-flip takes place even we consider the presence of only toroidal magnetic field in contrary to Refs. [15–19] where a poloidal component is considered. As mentioned in Sec. VI, this is due to the precision related issue involved with the MATLAB code that has been used in those studies. The default numerical precision of MATLAB was unable to deal with the smallness of the two dimensionless coefficients,  $V_m$  and  $V_B$ . We have corrected this issue in our new C++ code. A neutrino can undergo spin oscillations when it interacts with a magnetic field transverse to its velocity. One can see in Fig. 1(b) that there exist neutrinos which cross the accretion disk while the toroidal magnetic field is perpendicular to their momenta. Using such a qualitative argument, we conclude that only toroidal field can cause the neutrino spin-flip in the gravitational scattering. This finding of ours is promising since the toroidal magnetic field is inherent in the ‘‘Polish doughnut’’ model. Despite the fact that the helical magnetic fields, i.e. having both toroidal and poloidal components, provide the stabilization of astrophysical plasmas [44], there is no commonly accepted model for a poloidal field in accretion disks.

The next important improvement made in the present work in comparison to Refs. [15, 18] consists in the explicit separate descriptions of spin oscillations of upper and lower particles. Indeed, in Refs. [15, 18], we have computed the survival probability only for the upper particles and then reconstructed  $P_{LL}$  for the lower ones using the symmetry properties of the effective Hamiltonian in Eq. (51). It leads to the symmetric distributions of  $P_{LL}(\theta_{\text{obs}}, \phi_{\text{obs}})$  with respect to the  $\theta_{\text{obs}} = \pi/2$  reflection plane.

However, such a reflection symmetry with respect to the  $\theta_{\text{obs}} = \pi/2$  plane is valid only for purely gravitational interactions of neutrinos in the absence of the accretion disk. If one takes into account the neutrino interactions with the background matter and magnetic field,  $P_{LL}(\theta_{\text{obs}}, \phi_{\text{obs}})$  remains

symmetric only for a slowly rotating BH,  $a \ll 1$ , while the incoming neutrinos propagate parallel to the equatorial plane,  $|t_i| \ll 1$ . In all other cases,  $P_{LL}(\theta_{\text{obs}}, \phi_{\text{obs}})$  is not symmetric with respect to the  $\theta_{\text{obs}} = \pi/2$  plane. This feature can be seen in Figs. 6 and 7.

In the present work, we describe the spin oscillations of neutrinos for the arbitrary inclination of the incoming flux,  $0 < \theta_i < \pi$ . One can see in Figs. 6 and 7 that  $P_{LL}$  for the opposite values of  $t_i$  with the same BH spin are inversely symmetric only in the case of a slowly rotating BH,  $a \ll 1$ . This feature of  $P_{LL}$  disappears for a rapidly rotating BH. It means that it is an inherent property of the Kerr metric.

The study with a number of arbitrary  $\theta_i$ 's is motivated by the fact that, in some cases, the BH spin can be significantly inclined towards the galactic plane. For example, there are indirect indications in Ref. [26] that the spin of SMBH in our Galaxy is almost in the Galactic plane. If we study the gravitational scattering and spin oscillations of neutrinos, which are emitted in a SN explosion, by such a BH, our results shall be of great importance. Since we do not know the mutual position of a neutrino source and the Earth at the moment of the observation of the neutrino signal, one has to consider multiple values of  $\theta_i$ . In our work, we attempt to address this problem.

The next important result obtained in the present work is the consideration of both co-rotating and counter-rotating disks. Comparing Figs. 6 and 7, one can see that the observed fluxes of scattered neutrinos are different despite we consider the disks with equal maximal number densities of plasma and maximal strengths of the magnetic field. Thus, performing a precise measurement of astrophysical neutrinos that are gravitationally scattered by SMBH, one can potentially infer the information about the disk rotation direction.

## VIII. CONCLUSION

In this work, we consider the propagation of the ultra-relativistic neutrinos with nonzero magnetic moment in the strong gravitational field of a SMBH. The neutrinos are traveling at a random angle with respect to the equatorial plane of the SMBH. The SMBH is surrounded by a thick magnetized accretion disk. We consider those neutrinos that are scattered due to strong gravitational field of the SMBH since only such neutrinos can be observed. We can exactly describe the geodesic motion of these neutrinos in Kerr metric.

The neutrinos not only interact electroweakly with the rotating matter of the accretion disk, but also interact magnetically with the disk due to its nonzero magnetic moment. In this study, we consider only toroidal field inside the disk. The neutrino interaction with the external fields causes

the spin precession which can be accounted for along each neutrino trajectory. To have a good resolution of  $P_{LL}$  in the  $(\theta_{\text{obs}}, \phi_{\text{obs}})$  plane, we consider more than 2 million gravitationally scattered neutrinos in each combination of BH spin and incident angle.

The importance of our results is multi-fold. First, Figs. 6 and 7 show that it is enough to have the toroidal magnetic field, which is inherent in the ‘‘Polish doughnut’’ model, for spin oscillations to occur.

Second, we find that the symmetric distributions of  $P_{LL}(\theta_{\text{obs}}, \phi_{\text{obs}})$  with respect to the  $\theta_{\text{obs}} = \pi/2$  reflection plane can be seen either in the absence of the accretion disk or for a slowly rotating BH in the presence of the accretion disk. For all other cases, no such symmetry is observed.

Third, we observe that the inverse symmetry of  $P_{LL}$  for the opposite values of  $t_i (= \cos \theta_i)$  with the same BH spin is exhibited for a slowly rotating BH only. For a rapidly rotating BH, this inverse symmetry disappears. This points to the inherent property of the Kerr metric.

Fourth, since the relative position between a neutrino source and Earth is not known during the observation, our study carries important information due to the computation of  $P_{LL}$  for a number of arbitrary  $\theta_i$ 's.

Fifth, our results show the clear difference between the observed fluxes of scattered neutrinos for the co-rotating and counter-rotating disks (see Figs. 6 and 7). This can help in inferring the direction of the disk rotation in a precise measurement of astrophysical neutrinos that are gravitationally scattered by SMBH.

In addition to above, the obtained results can be useful in the neutrino tomography of magnetic fields and plasma distributions inside an accretion disk. There is always a probability that the scattered neutrinos, which undergo interactions with the background matter, magnetic and gravitational fields, can be emitted in a SN explosion in our Galaxy. According to the estimates in Ref. [15], the spin effects in such a case can be observed by the current or future neutrino telescopes (see, e.g., Ref. [45]).

#### ACKNOWLEDGMENTS

We thank A. F. Zakharov for useful discussion. All our numerical computations have been performed at Govorun super-cluster at Joint Institute for Nuclear Research, Dubna.

## Appendix A: Elliptic integrals and their useful relations

We follow the definitions of Elliptic integrals and functions as in Ref. [31]. In this Appendix, we provide some of the useful expressions.

The Incomplete Elliptic integral of first kind is defined as

$$F(\varphi, m) = \int_0^\varphi \frac{dx}{\sqrt{1 - m \sin^2 x}}. \quad (\text{A1})$$

If  $\varphi = \frac{\pi}{2}$ , we get the complete Elliptic integral of first kind in the form,

$$K(m) \equiv F\left(\frac{\pi}{2}, m\right) = \int_0^{\pi/2} \frac{dx}{\sqrt{1 - m \sin^2 x}}. \quad (\text{A2})$$

The Incomplete Elliptic integral of third kind is defined as,

$$\Pi(\varphi, n, m) = \int_0^\varphi \frac{dx}{(1 - n \sin^2 x) \sqrt{1 - m \sin^2 x}}. \quad (\text{A3})$$

If  $\varphi = \frac{\pi}{2}$ , we get the complete Elliptic integral of third kind,

$$\Pi(n, m) \equiv \Pi\left(\frac{\pi}{2}, n, m\right) = \int_0^{\pi/2} \frac{dx}{(1 - n \sin^2 x) \sqrt{1 - m \sin^2 x}}. \quad (\text{A4})$$

The functions  $F(\varphi, m)$  and  $K(m)$  obey the following properties:

$$\begin{aligned} F(\varphi, -m) &= \frac{1}{\sqrt{1+m}} \left[ K\left(\frac{m}{1+m}\right) - F\left(\frac{\pi}{2} - \varphi, \frac{m}{1+m}\right) \right], \\ K(-m) &= \frac{1}{\sqrt{1+m}} K\left(\frac{m}{1+m}\right), \end{aligned} \quad (\text{A5})$$

which can be derived from Eqs. (A1) and (A2).

## Appendix B: Explicit forms for various quantities

### 1. The components of gravi-electromagnetic field

The explicit form of  $\tilde{\mathbf{e}}_g$  and  $\tilde{\mathbf{b}}_g$  in Eq. (47) is given in [17]. These vectors are

$$\tilde{e}_{g1} = \frac{1}{2\sqrt{z^2 \cos^2 \theta (x^2 - x + z^2) + z^2 x^2 + z^2 x + x^4 (x^2 + z^2 \cos^2 \theta)^2}} \quad (\text{B1})$$

$$\begin{aligned} &\times \left\{ r_g \frac{d\phi}{dr} [z^3 \cos^4 \theta (z^2 - x^2) - z \cos^2 \theta (z^4 + 3x^4) + z^3 x^2 + 3zx^4] \right. \\ &\left. + \frac{dt}{dr} [z^2 \cos^2 \theta (z^2 + x^2) - z^2 x^2 - x^4] \right\}, \end{aligned} \quad (\text{B2})$$

$$\begin{aligned}\tilde{e}_{g2} &= \frac{z^2 x \sin 2\theta \sqrt{x^2 - x + z^2} \left[ \frac{dt}{dr} - r_g \frac{d\phi}{dr} z \sin^2 \theta \right]}{2\sqrt{z^2 \cos^2 \theta (x^2 - x + z^2) + z^2 x^2 + z^2 x + x^4 (x^2 + z^2 \cos^2 \theta)^2}}, \\ \tilde{e}_{g3} &= -\frac{\left[ z^2 x \sin 2\theta r_g \frac{d\theta}{dr} (x^2 - x + z^2) + z^2 \cos^2 \theta (z^2 - x^2) - z^2 x^2 - 3x^4 \right]}{2 \left[ z^4 \cos^4 \theta (x^2 - x + z^2) + x z^2 \cos^2 \theta (2z^2 x + 2x^3 - x^2 + z^2) + x^6 + z^2 x^4 + z^2 x^3 \right]} \\ &\quad \times \frac{z \sin \theta}{\sqrt{x^2 - x + z^2}},\end{aligned}\tag{B3}$$

$$\tilde{b}_{g1} = \frac{\cos \theta}{\sqrt{z^2 \cos^2 \theta (x^2 - x + z^2) + z^2 x^2 + z^2 x + x^4 (x^2 + z^2 \cos^2 \theta)^2}}\tag{B4}$$

$$\times \left\{ r_g \frac{d\phi}{dr} \left[ z^4 \cos^4 \theta (x^2 - x + z^2) + 2x^2 z^2 \cos^2 \theta (x^2 - x + z^2) + z^4 x + z^2 x^4 + 2z^2 x^3 + x^6 \right] \right.\tag{B5}$$

$$\left. - z x \frac{dt}{dr} (z^2 + x^2) \right\},$$

$$\tilde{b}_{g2} = -\frac{\sin \theta \sqrt{x^2 - x + z^2}}{2\sqrt{z^2 \cos^2 \theta (x^2 - x + z^2) + z^2 x^2 + z^2 x + x^4 (x^2 + z^2 \cos^2 \theta)^2}}\tag{B6}$$

$$\times \left\{ r_g \frac{d\phi}{dr} \left[ z^4 \cos^4 \theta (2x - 1) + z^2 \cos^2 \theta (z^2 + 4x^3 + x^2) + 2x^5 - z^2 x^2 \right] + z \frac{dt}{dr} (x^2 - z^2 \cos^2 \theta) \right\},$$

$$\tilde{b}_{g3} = \frac{z^2 \sin \theta \cos \theta + r_g \frac{d\theta}{dr} x (x^2 - x + z^2)}{\sqrt{x^2 - x + z^2} (x^2 + z^2 \cos^2 \theta)}.\tag{B7}$$

In Eq. (B1), the derivatives such as,  $\frac{d\phi}{dr}$  etc., can be calculated with the help of Eqs. (8) and (9).

However, we have to take into account the number of inversions of the trajectory. Thus, we get,

$$r_g \frac{d\theta}{dr} = (-1)^N \frac{\sqrt{w - (y^2 + w - z^2) \cos^2 \theta - z^2 \cos^4 \theta}}{\sin \theta \sqrt{x^4 + x^2 [z^2 - w - y^2] + x [w + (z - y)^2] - z^2 w}},\tag{B8}$$

$$r_g \frac{d\phi}{dr} = \pm \frac{z \sin^2 \theta (x - zy) + y (x^2 - x + z^2)}{\sin^2 \theta (x^2 - x + z^2) \sqrt{x^4 + x^2 [z^2 - w - y^2] + x [w + (z - y)^2] - z^2 w}},\tag{B9}$$

$$\frac{dt}{dr} = \pm \frac{z^2 \cos^2 \theta (x^2 - x + z^2) + z^2 x^2 + z^2 x + x^4 - xyz}{(x^2 + z^2 - x) \sqrt{x^4 + x^2 [z^2 - w - y^2] + x [w + (z - y)^2] - z^2 w}},\tag{B10}$$

where the signs  $\pm$  correspond to outgoing and incoming particles, and the number of inversions,  $N$ , is given in Eqs. (17), (23), (29) and (32).

## 2. The effective velocity

The components of the vector  $\mathbf{v}$ , used in Eq. (47), have the form,

$$v_1 = \pm \sqrt{x^4 + x^2 [z^2 - w - y^2] + x [w + (z - y)^2] - z^2 w}\tag{B11}$$

$$\times \frac{\sqrt{z^2 \cos^2 \theta (x^2 - x + z^2) + z^2 x^2 + z^2 x + x^4}}{z^2 \cos^2 \theta (x^2 - x + z^2) + z^2 x^2 + z^2 x + x^4 - xyz}, \quad (\text{B12})$$

$$v_2 = \pm (-1)^N \sqrt{w - (y^2 + w - z^2) \cos^2 \theta - z^2 \cos^4 \theta} \quad (\text{B13})$$

$$\times \frac{\sqrt{z^2 + x^2 - x} \sqrt{z^2 \cos^2 \theta (x^2 - x + z^2) + z^2 x^2 + z^2 x + x^4}}{\sin \theta [z^2 \cos^2 \theta (x^2 - x + z^2) + z^2 x^2 + z^2 x + x^4 - xyz]}, \quad (\text{B14})$$

$$v_3 = \frac{y \{ (x^2 + z^2 \cos^2 \theta - x) [z^2 \cos^2 \theta (x^2 - x + z^2) + z^2 x^2 + z^2 x + x^4] + x^2 z^2 \sin^2 \theta \}}{\sin \theta (x^2 + z^2 \cos^2 \theta) \sqrt{x^2 - x + z^2} [z^2 \cos^2 \theta (x^2 - x + z^2) + z^2 x^2 + z^2 x + x^4 - xyz]}. \quad (\text{B15})$$

The quantity  $u^0$  reads

$$\frac{u^0}{U^t} = \frac{\sqrt{z^2 \cos^2 \theta + x^2} \sqrt{z^2 + x^2 - x}}{\sqrt{z^2 \cos^2 \theta (x^2 - x + z^2) + z^2 x^2 + z^2 x + x^4}}. \quad (\text{B16})$$

We do not provide the components of the four vector  $l^a$ ,  $l^0 = \frac{dt}{dr} \frac{u^0}{U^t}$  and  $\mathbf{l} = \frac{dt}{dr} \frac{u^0}{U^t} \mathbf{v}$  here, since they can be computed based on Eqs. (B8)-(B16).

### 3. The effective potential of the neutrino interaction with background matter

From Eq. (54), we can write the nonzero components of the four vector  $g^a = (g^0, 0, 0, g^3)$  as,

$$g^0 = \frac{\sqrt{x^2 + z^2 \cos^2 \theta} \sqrt{x^2 - x + z^2} U_f^t}{\sqrt{z^2 \cos^2 \theta (x^2 - x + z^2) + z^2 x^2 + z^2 x + x^4}},$$

$$g^3 = \frac{\sin \theta \left[ r_g U_f^\phi (z^2 \cos^2 \theta (x^2 - x + z^2) + z^2 x^2 + z^2 x + x^4) - U_f^t x z \right]}{\sqrt{x^2 + z^2 \cos^2 \theta} \sqrt{z^2 \cos^2 \theta (x^2 - x + z^2) + z^2 x^2 + z^2 x + x^4}}. \quad (\text{B17})$$

We use the above forms of  $g^0$  and  $g^3$  in Eq. (49) to compute  $\Omega_x^{\text{matt}}$ .

### 4. Toroidal magnetic field in the locally Minkowskian frame

The only nonzero component of the electromagnetic field in the locally Minkowskian frame, which contributes to Eq. (48), is

$$b_3 = - \frac{U_f^t r_g^2 \sqrt{2p_m}}{\sin \theta (1 - \Omega l_0) \sqrt{(x^2 + z^2 \cos^2 \theta)(x^2 - x + z^2)}} \times \{ \lambda_0^2 (x^2 - x + z^2 \cos^2 \theta) + 2\lambda_0 x z \sin^2 \theta - \sin^2 \theta [(x^2 + z^2)(x^2 + z^2 \cos^2 \theta) + x z^2 \sin^2 \theta] \}^{1/2}, \quad (\text{B18})$$

where  $\lambda_0 = l_0/r_g$ .

### Appendix C: Adam-Bashforth and Adam-Moulton Multi-step methods

We discuss the solution of a first order differential equation

$$\frac{dy}{dx} = f(y(x), x). \quad (C1)$$

The function  $f$  is known only at discrete and irregularly spaced points,  $i$ . Due to this, we use 4th order Adam-Bashforth predictor method for approximate solution, and then we use 4th order Adam-Moulton corrector method to improve the obtained solution.

For a 4th order solution, we can write for Adam-Bashforth method as,

$$y_{i+4} = y_{i+3} + C_3^{\text{AB}} f_{i+3} + C_2^{\text{AB}} f_{i+2} + C_1^{\text{AB}} f_{i+1} + C_0^{\text{AB}} f_i, \quad (C2)$$

where the coefficients are defined as,

$$\begin{aligned} C_3^{\text{AB}} &= \frac{1}{12(x_i - x_{i+3})(x_{i+2} - x_{i+3})(x_{i+1} - x_{i+3})} \\ &\quad [3x_{i+3}^4 - 4(x_i + x_{i+1} + x_{i+2})x_{i+3}^3 \\ &\quad + \{(6x_i + 6x_{i+2})x_{i+1} + 6x_i x_{i+2}\}x_{i+3}^2 - 12x_i x_{i+1} x_{i+2} x_{i+3} \\ &\quad + \{(12x_i x_{i+4} - 6x_{i+4}^2)x_{i+2} - 6x_i x_{i+4}^2 + 4x_{i+4}^3\}x_{i+1} \\ &\quad + (-6x_i x_{i+4}^2 + 4x_{i+4}^3)x_{i+2} + 4x_i x_{i+4}^3 - 3x_{i+4}^4], \end{aligned} \quad (C3)$$

$$C_2^{\text{AB}} = \frac{(x_{i+3} - x_{i+4})^2}{12(x_i - x_{i+2})(x_{i+1} - x_{i+2})(x_{i+2} - x_{i+3})} \frac{6x_i x_{i+1} - 2x_i x_{i+3} - 4x_i x_{i+4} - 2x_{i+1} x_{i+3} - 4x_{i+1} x_{i+4} + x_{i+3}^2 + 2x_{i+3} x_{i+4} + 3x_{i+4}^2}{}, \quad (C4)$$

$$C_1^{\text{AB}} = \frac{-(x_{i+3} - x_{i+4})^2}{12(x_i - x_{i+1})(x_{i+1} - x_{i+3})(x_{i+1} - x_{i+2})} \frac{6x_i x_{i+2} - 2x_i x_{i+3} - 4x_i x_{i+4} - 2x_{i+2} x_{i+3} - 4x_{i+2} x_{i+4} + x_{i+3}^2 + 2x_{i+3} x_{i+4} + 3x_{i+4}^2}{}, \quad (C5)$$

$$C_0^{\text{AB}} = \frac{(x_{i+3} - x_{i+4})^2}{12(x_i - x_{i+3})(x_i - x_{i+2})(x_i - x_{i+1})} \frac{6x_{i+1} x_{i+2} - 2x_{i+1} x_{i+3} - 4x_{i+1} x_{i+4} - 2x_{i+2} x_{i+3} - 4x_{i+2} x_{i+4} + x_{i+3}^2 + 2x_{i+3} x_{i+4} + 3x_{i+4}^2}{}. \quad (C6)$$

We then use the solution obtained from the Adam-Bashforth method into Adam-Moulton corrector method which can be written as,

$$y_{i+4} = y_{i+3} + C_4^{\text{AM}} f_{i+4} + C_3^{\text{AM}} f_{i+3} + C_2^{\text{AM}} f_{i+2} + C_1^{\text{AM}} f_{i+1}, \quad (C7)$$

where,

$$C_4^{\text{AM}} = \frac{(x_{i+4} - x_{i+3})(6x_{i+1}x_{i+2} - 2x_{i+1}x_{i+3} - 4x_{i+1}x_{i+4} - 2x_{i+2}x_{i+3} - 4x_{i+2}x_{i+4} + x_{i+3}^2 + 2x_{i+3}x_{i+4} + 3x_{i+4}^2)}{12(x_{i+2} - x_{i+4})(x_{i+1} - x_{i+4})}, \quad (\text{C8})$$

$$C_3^{\text{AM}} = \frac{(x_{i+4} - x_{i+3})(6x_{i+1}x_{i+2} - 4x_{i+1}x_{i+3} - 2x_{i+1}x_{i+4} - 4x_{i+2}x_{i+3} - 2x_{i+2}x_{i+4} + 3x_{i+3}^2 + 2x_{i+3}x_{i+4} + x_{i+4}^2)}{12(x_{i+2} - x_{i+3})(x_{i+1} - x_{i+3})}, \quad (\text{C9})$$

$$C_2^{\text{AM}} = \frac{(2x_{i+1} - x_{i+3} - x_{i+4})(x_{i+3} - x_{i+4})^3}{12(x_{i+2} - x_{i+4})(x_{i+2} - x_{i+3})(x_{i+1} - x_{i+2})}, \quad (\text{C10})$$

$$C_1^{\text{AM}} = -\frac{(2x_{i+2} - x_{i+3} - x_{i+4})(x_{i+3} - x_{i+4})^3}{12(x_{i+1} - x_{i+4})(x_{i+1} - x_{i+3})(x_{i+1} - x_{i+2})}. \quad (\text{C11})$$

We then use the Eqs. (C2) and (C7) to solve Eq. (50) as described in Sec. IV.

## REFERENCES

- 
- [1] V. A. Allakhverdyan, et al. (Baikal Collaboration), “Diffuse neutrino flux measurements with the Baikal-GVD neutrino telescope,” *Phys. Rev. D* **107**, 042005 (2023) doi:10.1103/PhysRevD.107.042005 [arXiv:2211.09447].
  - [2] R. Abbasi, et al. (IceCube Collaboration), “Observation of Seven Astrophysical Tau Neutrino Candidates with IceCube,” *Phys. Rev. Lett.* **132**, 151001 (2024) doi:10.1103/PhysRevLett.132.151001 [arXiv:2403.02516].
  - [3] R. Abbasi, et al., “IceCube Search for Neutrinos Coincident with Gravitational Wave Events from LIGO/Virgo Run O3,” *Astrophys. J.* **944**, 80 (2023) doi:10.3847/1538-4357/aca5fc [arXiv:2208.09532].
  - [4] K. Fujikawa and R. Shrock, “The Magnetic Moment of a Massive Neutrino and Neutrino Spin Rotation,” *Phys. Rev. Lett.* **45**, 963 (1980) doi:10.1103/PhysRevLett.45.963.
  - [5] C. Giunti, K. A. Kouzakov, Y.-F. Li, A. V. Lokhov, A. I. Studenikin, and S. Zhou, “Electromagnetic neutrinos in laboratory experiments and astrophysics,” *Ann. Phys. (Berlin)* **528**, 198 (2016) doi:10.1002/andp.201500211 [arXiv:1506.05387].
  - [6] A. Papapetrou, “Spinning test particles in general relativity. 1.,” *Proc. Roy. Soc. Lond. A* **209**, 248-258 (1951) doi:10.1098/rspa.1951.0200.

- [7] S. N. Vergeles, N. N. Nikolaev, Yu. N. Obukhov, A. Ya. Silenko, and O. V. Teryaev, “General relativity effects in precision spin experimental tests of fundamental symmetries,” *Phys. Usp.* **66**, 109–147 (2023) doi:10.3367/UFNr.2021.09.039074 [arXiv:2204.00427].
- [8] M. Dvornikov, “Neutrino spin oscillations in gravitational fields,” *Int. J. Mod. Phys. D* **15**, 1017-1034 (2006) doi:10.1142/S021827180600870X [arXiv:hep-ph/0601095 [hep-ph]].
- [9] M. Dvornikov, “Neutrino spin oscillations in matter under the influence of gravitational and electromagnetic fields,” *JCAP* **06**, 015 (2013) doi:10.1088/1475-7516/2013/06/015 [arXiv:1306.2659 [hep-ph]].
- [10] S. A. Alavi and S. Nodeh, “Neutrino spin oscillations in gravitational fields in noncommutative spaces,” *Phys. Scripta* **90**, no.3, 035301 (2015) doi:10.1088/0031-8949/90/3/035301 [arXiv:1301.5977 [gr-qc]].
- [11] S. Chakraborty, “Aspects of Neutrino Oscillation in Alternative Gravity Theories,” *JCAP* **10**, 019 (2015) doi:10.1088/1475-7516/2015/10/019 [arXiv:1506.02647 [gr-qc]].
- [12] L. Mastrototaro and G. Lambiase, “Neutrino spin oscillations in conformally gravity coupling models and quintessence surrounding a black hole,” *Phys. Rev. D* **104**, no.2, 024021 (2021) doi:10.1103/PhysRevD.104.024021 [arXiv:2106.07665 [gr-qc]].
- [13] S. A. Alavi and T. F. Serish, “Neutrino spin oscillations in gravitational fields in higher dimensions,” *Mod. Phys. Lett. A* **37**, no.30, 2250200 (2022) doi:10.1142/S0217732322502005 [arXiv:2206.01940 [gr-qc]].
- [14] R. C. Pantig, L. Mastrototaro, G. Lambiase and A. Övgün, “Shadow, lensing, quasinormal modes, greybody bounds and neutrino propagation by dyonic ModMax black holes,” *Eur. Phys. J. C* **82**, no.12, 1155 (2022) doi:10.1140/epjc/s10052-022-11125-y [arXiv:2208.06664 [gr-qc]].
- [15] M. Dvornikov, “Gravitational scattering of spinning neutrinos by a rotating black hole with a slim magnetized accretion disk,” *Class. Quant. Grav.* **40**, no.1, 015002 (2023) doi:10.1088/1361-6382/aca45a [arXiv:2206.00042 [hep-ph]].
- [16] M. Dvornikov, “Neutrino Spin and Flavor Oscillations in Gravitational Fields,” *Phys. Part. Nucl. Lett.* **20**, no.3, 461-465 (2023) doi:10.1134/S154747712303024X [arXiv:2304.03622 [hep-ph]].
- [17] M. Dvornikov, “Scattering of neutrinos by a rotating black hole accounting for the electroweak interaction with an accretion disk,” *Int. J. Mod. Phys. D* **33**, no.14, 2340001 (2024) doi:10.1142/S0218271823400011 [arXiv:2212.03479 [hep-ph]].
- [18] M. Dvornikov, “Neutrino spin oscillations in a magnetized Polish doughnut,” *JCAP* **09**, 039 (2023) doi:10.1088/1475-7516/2023/09/039 [arXiv:2307.10126 [astro-ph.HE]].
- [19] M. Deka and M. Dvornikov, “Spin Oscillations in Neutrino Gravitational Scattering,” *Phys. Atom. Nucl.* **87**, no.4, 483-488 (2024) doi:10.1134/S1063778824700327 [arXiv:2311.14475 [hep-ph]].
- [20] K. Akiyama *et al.* [Event Horizon Telescope], “First M87 Event Horizon Telescope Results. I. The Shadow of the Supermassive Black Hole,” *Astrophys. J. Lett.* **875**, L1 (2019) doi:10.3847/2041-8213/ab0ec7 [arXiv:1906.11238 [astro-ph.GA]].
- [21] K. Akiyama *et al.* [Event Horizon Telescope], “First Sagittarius A\* Event Horizon Telescope Results. I. The Shadow of the Supermassive Black Hole in the Center of the Milky Way,” *Astrophys. J. Lett.*

- 930**, no.2, L12 (2022) doi:10.3847/2041-8213/ac6674 [arXiv:2311.08680 [astro-ph.HE]].
- [22] V. I. Dokuchaev and N. O. Nazarova, “Silhouettes of invisible black holes,” *Usp. Fiz. Nauk* **190**, no.6, 627-647 (2020) doi:10.3367/UFNe.2020.01.038717 [arXiv:1911.07695 [gr-qc]].
- [23] W. X. Chen and A. M. Beloborodov, “Neutrino-Cooled Accretion Disks around Spinning Black Hole,” *Astrophys. J.* **657**, 383-399 (2007) doi:10.1086/508923 [arXiv:astro-ph/0607145 [astro-ph]].
- [24] B. C. Bromley, K. Chen and W. A. Miller, “Line emission from an accretion disk around a rotating black hole: toward a measurement of frame dragging,” *Astrophys. J.* **475**, 57 (1997) doi:10.1086/303505 [arXiv:astro-ph/9601106 [astro-ph]].
- [25] O. Mena, I. Mocioiu and C. Quigg, “Gravitational Lensing of Supernova Neutrinos,” *Astropart. Phys.* **28**, 348-356 (2007) doi:10.1016/j.astropartphys.2007.07.002 [arXiv:astro-ph/0610918 [astro-ph]].
- [26] K. Akiyama *et al.* [Event Horizon Telescope], “First Sagittarius A\* Event Horizon Telescope Results. V. Testing Astrophysical Models of the Galactic Center Black Hole,” *Astrophys. J. Lett.* **930**, no.2, L16 (2022) doi:10.3847/2041-8213/ac6672 [arXiv:2311.09478 [astro-ph.HE]].
- [27] Abramowicz, M., Jaroszynski, M., Sikora, M., “Relativistic, accreting disk,” *Astronomy and Astrophysics* **63**, 221 (1978).
- [28] S. S. Komissarov, “Magnetized Tori around Kerr Black Holes: Analytic Solutions with a Toroidal Magnetic Field,” *Mon. Not. Roy. Astron. Soc.* **368**, 993-1000 (2006) doi:10.1111/j.1365-2966.2006.10183.x [arXiv:astro-ph/0601678 [astro-ph]].
- [29] S. Chandrasekhar, *The Mathematical Theory of Black Holes*, (Clarendon, Oxford, 1983).
- [30] S. E. Gralla, A. Lupsasca and A. Strominger, “Observational Signature of High Spin at the Event Horizon Telescope,” *Mon. Not. Roy. Astron. Soc.* **475**, no.3, 3829-3853 (2018) doi:10.1093/mnras/sty039 [arXiv:1710.11112 [astro-ph.HE]].
- [31] M. Abramowitz and I. Stegun, *Handbook of Mathematical Functions: with Formulas, Graphs, and Mathematical Tables* (National Bureau of Standards, Washington D.C., 1964).
- [32] V. Bargmann, L. Michel and V. L. Telegdi, “Precession of the polarization of particles moving in a homogeneous electromagnetic field,” *Phys. Rev. Lett.* **2**, 435-436 (1959) doi:10.1103/PhysRevLett.2.435.
- [33] M. Dvornikov and A. Studenikin, “Neutrino spin evolution in presence of general external fields,” *JHEP* **09**, 016 (2002) doi:10.1088/1126-6708/2002/09/016 [arXiv:hep-ph/0202113 [hep-ph]].
- [34] R. M. Wald, “Gravitational spin interaction,” *Phys. Rev. D* **6**, 406-413 (1972) doi:10.1103/PhysRevD.6.406.
- [35] I. B. Khriplovich and A. A. Pomeransky, “Equations of motion of spinning relativistic particle in external fields,” *J. Exp. Theor. Phys.* **86**, 839-849 (1998) doi:10.1134/1.558554 [arXiv:gr-qc/9710098 [gr-qc]].
- [36] F. Sorge and S. Zilio, “Neutrino spin flip around a Schwarzschild black hole,” *Class. Quant. Grav.* **24**, 2653-2664 (2007) doi:10.1088/0264-9381/24/10/011.
- [37] Y. N. Obukhov, A. J. Silenko and O. V. Teryaev, “General treatment of quantum and classical spinning particles in external fields,” *Phys. Rev. D* **96**, no.10, 105005 (2017) doi:10.1103/PhysRevD.96.105005

- [arXiv:1708.05601 [hep-th]].
- [38] M. A. Abramowicz and P. C. Fragile, “Foundations of Black Hole Accretion Disk Theory,” *Living Rev. Rel.* **16**, 1 (2013) doi:10.12942/lrr-2013-1 [arXiv:1104.5499 [astro-ph.HE]].
- [39] J. M. Bardeen, W. H. Press and S. A. Teukolsky, “Rotating black holes: Locally nonrotating frames, energy extraction, and scalar synchrotron radiation,” *Astrophys. J.* **178**, 347 (1972) doi:10.1086/151796
- [40] N. Viaux, M. Catelan, P. B. Stetson, G. Raffelt, J. Redondo, A. A. R. Valcarce and A. Weiss, “Particle-physics constraints from the globular cluster M5: Neutrino Dipole Moments,” *Astron. Astrophys.* **558**, A12 (2013) doi:10.1051/0004-6361/201322004 [arXiv:1308.4627 [astro-ph.SR]].
- [41] J. Jiang, A. C. Fabian, T. Dauser, L. Gallo, J. A. Garcia, E. Kara, M. L. Parker, J. A. Tomsick, D. J. Walton and C. S. Reynolds, “High Density Reflection Spectroscopy – II. The density of the inner black hole accretion disc in AGN,” *Mon. Not. Roy. Astron. Soc.* **489**, no.3, 3436-3455 (2019) doi:10.1093/mnras/stz2326 [arXiv:1908.07272 [astro-ph.HE]].
- [42] V. S. Beskin, “MHD Flows in Compact Astrophysical Objects: Accretion, Winds and Jets,” Springer, 2010, ISBN 978-3-642-01289-1, 978-3-642-01290-7 doi:10.1007/978-3-642-01290-7, p. 184.
- [43] M. Deka and M. Dvornikov, Neutrino spin oscillations near a black hole, submitted to *Phys. Atom. Nucl.*
- [44] S. Candelaresi and F. Del Sordo, “Stability of Plasmas Through Magnetic Helicity,” in *Helicities in Geophysics, Astrophysics, and Beyond*, ed. by K. Kuzanyan, N. Yokoi, M. K. Georgoulis, and R. Stepanov (Wiley, Hoboken, 2023), pp. 179–188.
- [45] A. Abusleme *et al.* [JUNO], “JUNO physics and detector,” *Prog. Part. Nucl. Phys.* **123**, 103927 (2022) doi:10.1016/j.pnpnp.2021.103927 [arXiv:2104.02565 [hep-ex]].